CMI Graduate Student Projects: Volume 1

Characterizing Bacterial Communities in Beaufort Sea Sediments in a Changing Arctic

Alexis Walker
College of Fisheries and Ocean Science, University of Alaska Fairbanks

---

Chukchi-Beaufort Seas Storms and Their Influence on Surface Climate

Yang Yang
International Arctic Research Center, University of Alaska Fairbanks

---

Using Genotyping-by-Sequencing (GBS) Population Genetics Approaches to Determine the Population Structure of Tanner Crab (*Chionoecetes bairdi*) in Alaska

Genevieve Johnson
College of Fisheries and Ocean Science, University of Alaska Fairbanks

March 2018
OCS Study BOEM 2018-021

BOEM
Bureau of Ocean Energy Management

UAF
University of Alaska Fairbanks

Contact Information:
Email: UAF-CMI@alaska.edu
phone: 907.474.6782

Coastal Marine Institute
College of Fisheries and Ocean Sciences
University of Alaska Fairbanks
P. O. Box 757220
Fairbanks, AK 99775-7220

These studies were funded in part by the U.S. Department of the Interior, Bureau of Ocean Energy Management (BOEM) under cooperative agreements M16AC00004, M16AC00007, and M16AC00011, between BOEM, Alaska Outer Continental Shelf Region, and the University of Alaska Fairbanks. This report, BOEM 2018-021 is available through the Coastal Marine Institute, select federal depository libraries, and electronically from *https://www.boem.gov/BOEM-Newsroom/Library/Publications/Alaska-Scientific-and-Technical-Publications.aspx*

Table of Contents

Characterizing Bacterial Communities in Beaufort Sea Sediments in a Changing Arctic

Principal Investigator: Alexis Walker

College of Fisheries and Ocean Sciences
University of Alaska Fairbanks

Cooperative Agreement Number: M16AC00004
Period of Performance: 6/16-1/18

Contents

List of Figures

List of Tables

Abstract

Reduced sea ice cover has shifted marine productivity patterns in the Arctic. These shifts affect the quality and quantity of organic matter (OM) deposited to the seafloor and available to the benthic organisms that rely on sinking material from overlying water masses for sustenance. Additionally, processes regulating the local remineralization and degradation of OM may be impacted. Sediment bacteria are the biogeochemical engineers of the benthos and play a vital role in OM and biogeochemical budgets. Although bacterial diversity and community structure can reflect local biogeochemical processes, environmental characteristics, physical disturbances, and chemical contaminants, they are largely understudied in the Beaufort Sea benthos. The overall goals of this study were to characterize broad-scale patterns in the diversity and community structure of benthic bacteria from the western Beaufort Sea into the Amundsen Gulf and to elucidate the environmental drivers of these patterns. To achieve these goals, sediment bacterial communities were characterized via the 16S rRNA gene using a next-generation DNA sequencing (NGS) approach. Diversity, community structure, and associated environmental correlates were assessed for 79 sampling sites across the Alaskan and Canadian regions of the Beaufort Sea shelf and slope to the Amundsen Gulf. Bacterial alpha-diversity exhibits overall positive correlations with depth, salinity, and $\delta^{15}N$ and negative correlations with chl-*a*, chl-*a*/phaeopigments, and C/N across all sediments analyzed. Patterns of beta-diversity are not highly definitive, and bacterial communities appear to be loosely clustered with high overlap in nMDS ordination space. Overall, bacterial communities are more similar within Beaufort sub-regions including the Alaskan Beaufort Shelf, the Mackenzie Shelf, Amundsen Gulf, and Banks Island. Environmental variables identified as drivers of community structure differences were depth, salinity, $\delta^{15}N$, chl-*a*, C/N, and total organic carbon (TOC). As previously ice-covered Arctic waters become more accessible for human activities, particularly petroleum and gas exploration, there is an increased likelihood of contaminant exposure. Our study area included samples within and adjacent to areas with high oil and gas resource potential. In order to gain a general sense of oil biodegradation potential across the study area, bacterial community data generated were queried for putative oil-degrading taxa. Of the 14 taxa investigated, the majority were found sporadically throughout the study area, with more taxa found on the Alaskan Beaufort Shelf and the Amundsen Gulf than on the Mackenzie Shelf. Only three taxa were ubiquitously distributed across all samples.

Introduction

Bacteria represent a biological link between the abiotic and biotic realms because their diverse metabolic pathways make them key mediators of biogeochemical processes. Unlike higher trophic level organisms, bacteria can metabolize both organic and inorganic compounds, making them essential in the replenishment and removal of nutrients to surrounding organisms. For example, benthic organisms that feed on sinking material must deal with the challenge of obtaining nutrition from a food source that has been degraded during transport through the overlying water column (Arndt et al., 2013; Lopez & Levinton, 1987). Bacteria in sediments metabolize these degraded compounds and produce more labile material for neighboring micro- and meio-fauna (as byproducts of metabolism or by becoming food for benthic organisms). Additionally, bacteria can sequester labile organic material and remove nutrients from the benthic system via assimilation and mortality. Thus, bacteria play an integral role in nutrient and OM degradation and cycling and contribute to fluxes of energy throughout the benthic food web (Bienhold, Boetius, & Ramette, 2012a; Deming & Baross, 1993). Particular bacterial taxonomic groups metabolize specific compounds. For example, in Arctic marine sediments, the bacterial taxa *Flavobacteria, Marinilabiaceae, and Pseudoalteromonadaceae* exhibit a strong positive correlation and increase in relative abundance with increased nutrients and fresh phytodetritus. Moreover, bacterial diversity generally increases with increased phytodetritus flux (Bienhold, Boetius, & Ramette, 2012a). Bacterial taxa such as *Acidobacteria* can also indicate nutrient-poor conditions (Bienhold, Boetius, & Ramette, 2012a; Teske et al., 2011). Therefore, bacterial diversity and community composition may provide insight into the quantity and quality of material deposited from surface primary production and the local pool of OM and nutrients available to benthic consumers (Judd, Crump, & Kling, 2006).

The study area covers a broad geographical range from the western Beaufort Sea near the Colville River to the Amundsen Gulf and Banks Island. This Arctic sector encompasses three large regions: the Alaskan Beaufort Shelf (ABS), the Mackenzie Shelf (MS), and the Amundsen Gulf (AG) (Figure 1). The Amundsen Gulf is a large channel connecting the Canadian Arctic Archipelago with the southeast Beaufort Sea, bordered by the Mackenzie Shelf to the southwest and Banks Island (BI) to the north. The Amundsen Gulf is characterized by a narrow shelf, several peripheral bays, straights, and inlets, and a central basin with an average depth of 300 m and a maximum depth of 630 m (Forest et al., 2010; Gamboa et al., 2017; Stokes, Clark, & Winsborrow, 2006). The Mackenzie Shelf is characterized by inner, middle, and outer shelf regions with depths 0–45, 45–80, and 80–100 m, respectively (Carmack & Macdonald, 2002). Bordered by the Mackenzie Canyon to the west and the Amundsen Gulf trough to the east, the Mackenzie Shelf has been described as a vast estuary because its water properties are greatly influenced by both coastal (Mackenzie River) and marine sources (Arctic Ocean) (Carmack & Macdonald, 2002; Magen et al., 2010). The Mackenzie River, fourth largest in the Arctic in terms of freshwater discharge and the largest in terms of sediment transport, greatly influences the water and sediment characteristics of the Mackenzie Shelf and, to a lesser extent, the eastern-most section of the Alaskan Beaufort Shelf and Amundsen Gulf (Rachold et al., 2004). Several

smaller sporadic rivers flowing from the Alaskan coastline also influence the Alaskan Beaufort Shelf. The Alaskan Beaufort Shelf is bordered by Point Barrow to the west and the Mackenzie Canyon to the east, with a shelf break at ~80 m water depth. The water properties of the Alaskan Beaufort Shelf are also influenced by warmer Bering Strait water, referred to as the Beaufort shelf-break jet, which flows due east from Barrow Canyon (Dunton, Weingartner, & Carmack, 2006; Pickart, 2004).

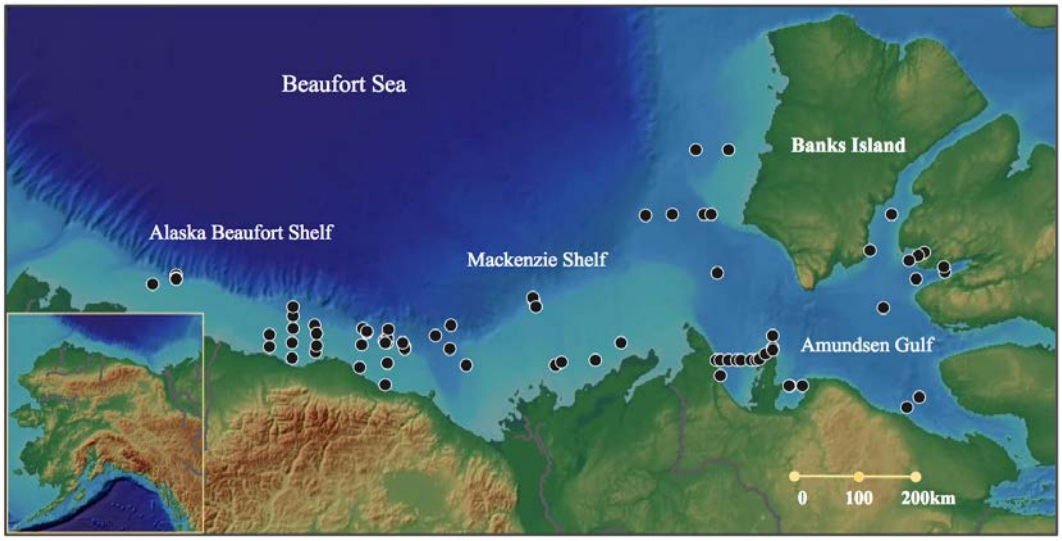

Figure 1. Map of the study area including sample stations and regions defined by certain oceanographic characteristics.

The environmental gradients exhibited in the study area provide a natural experimental setting for exploration of linkages between environmental characteristics and bacterial community structure. Identifying links between bacterial community composition and function is a growing area of research aimed at identifying ecologically important bacterial groups (Fuhrman, 2009; Teske et al., 2011). Arctic benthic bacterial communities have only been explored in a handful of studies, with the majority conducted prior to 1980 or in deep-sea sediments in Greenland and Norway (e.g., Bienhold, Boetius, & Ramette, 2012b; Buttigieg & Ramette, 2015; Jacob et al., 2013; Teske et al., 2011). Multiple studies have characterized pelagic bacteria in the Beaufort Sea; however, pelagic and benthic bacterial communities are significantly different with respect to composition, diversity, and function (e.g., Ortega-Retuerta et al., 2013; Zinger et al., 2011). Biogeographical patterns of community composition and diversity have already been established for bacterial communities in deep-sea Arctic sediments where environmental conditions are relatively uniform and constant (Buttigieg & Ramette, 2015; Jacob et al., 2013). Therefore, it is likely that the wide range of benthic habitat conditions across the Beaufort Sea and the Amundsen Gulf will be reflected in sediment bacterial community structure and diversity.

Benthic bacteria are valuable bioindicators because they reflect both short-term and long-term environmental changes. In the long term, community structure remains relatively constant, mirroring trends in environmental characteristics such as food availability, hydrography, and

bathymetry (Zinger et al., 2011). Bacteria can also be considered the microbial equivalent to the "canary in the coal mine" due to high turnover rates and immediate and successive shifts in community structure following a disturbance. Shifts in bacterial community structure may also indicate the presence of contaminants such as heavy metals and hydrocarbons, which are chemical components of crude oil, in the environment. A variety of bacterial taxa involved in oil biodegradation, including some obligate oil-degraders, occur naturally in low or undetectable numbers prior to a large oil exposure event. These taxa, which typically "bloom" following oil exposure, can rapidly break down the chemical components of oil *in situ* (Head, Jones, & Röling, 2006; McKew et al., 2007; Yakimov, Timmis, & Golyshin, 2007). The effectiveness and efficiency with which these bacteria can degrade oil increases significantly with diversity (Dell'Anno et al., 2012; McKew et al., 2007; Röling et al., 2002). Higher bacterial diversity translates to more metabolic strategies available to break down complex compounds in oil and the resulting degradation products. Establishing the presence and distribution of known oil-degrading taxa and associated community diversity provides valuable insights into how microbial communities might respond to oil exposure in a given location (Dell'Anno et al., 2012). This information is particularly relevant in the study area, which incorporates regions within and adjacent to areas with current and historical exploratory oil and natural gas wells and areas designated as having high oil and gas resource potential in the Beaufort Sea (Figure 2) (BOEM, 2012; CAFF/USGS, 2017).

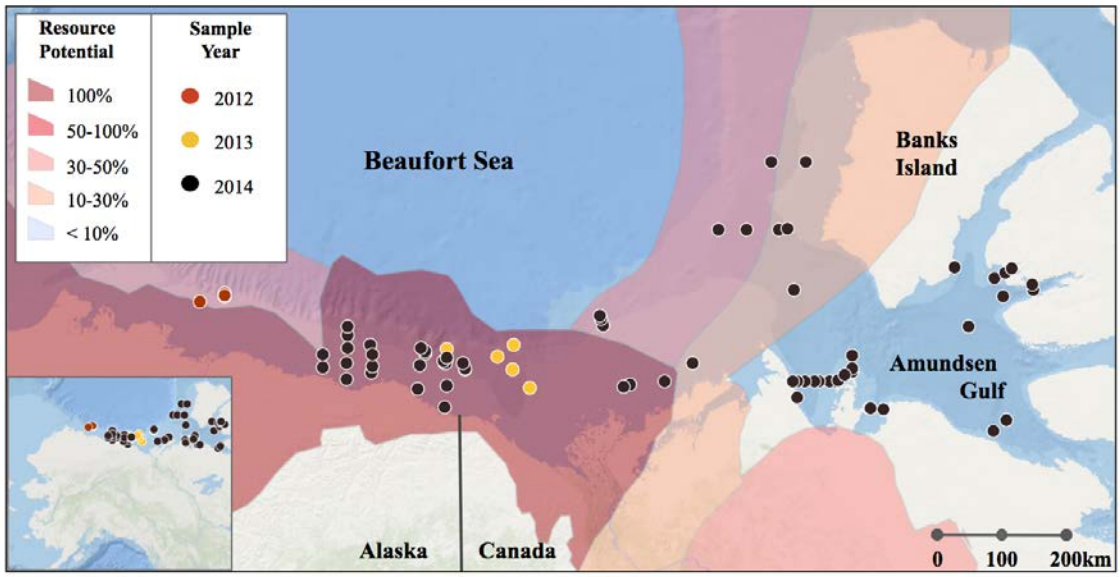

Figure 2. Map of the 79 sampling locations across the Beaufort Sea and the Amundsen Gulf relative to oil and gas potential. Sediments for bacterial community analyses were collected in 2012, 2013, and 2014. The areas of oil and gas potential represent the percent likelihood of the presence of oil/gas and gas reserves, with 100% being areas where the presence of oil/gas has been established through exploratory drilling (CAFF/USGS, 2017).

Objectives

1. Assess the diversity and community structure of sediment bacteria at 79 locations distributed across the Beaufort Sea continental shelf and slope.
2. Examine correlations between environmental parameters and corresponding bacterial diversity and community composition.
3. Query bacterial community composition from 79 sediment samples for potential oil-degrading taxa.

Methods

Sample Collection

A total of 79 archived sediment samples were processed and sequenced using next-generation sequencing (NGS). The resulting data were analyzed using multivariate statistics. Samples were collected opportunistically in 2012–2014 across a broad section of the Beaufort Sea and Amundsen Gulf (~151–119°W) as part of two collaborative field programs, the US-Transboundary Fish and Lower Trophic Communities Project (USTB) and the Beaufort Regional Environmental Assessment Project (BREA). Sampling efforts included a series of shelf-slope transects starting near the Colville River and extending to the Amundsen Gulf and northward near Banks Island at 20 –1200 m depths (Figure 1). All sediment samples, environmental and genomic, were collected from the top 1 cm surface layer of a double van Veen grab (USTB 2014) or a 0.25 m^2 box core sample (USTB 2012 and BREA) using a 60 cc (2.5 cm) sterilized syringe. Following collection aboard respective vessels, the samples were immediately frozen at -20^{o}C and stored at -80^{o}C upon arrival at UAF.

Sediment Characteristics

Seven sediment characteristics were used to investigate correlations with bacterial diversity and community structure: Chlorophyll-*a* concentration (chl-*a*), phaeopigments concentration (phaeo), chl-*a:* phaeopigments (Ch/Ph), total organic carbon (TOC), carbon:nitrogen (C/N), $\delta^{13}C$, and $\delta^{15}N$. These characteristics include commonly used proxies for the quality and quantity of organic matter in sediments. All parameters were measured on sediment samples taken from the upper 1 cm of either the same box core or replicate grab samples from the same stations as the bacterial genomic samples. Additional environmental variables included depth, bottom water temperature, and bottom water salinity recorded from CTD profiles at each station. All environmental data were collected as part of the USTB and BREA field programs (S. Hardy-USTB, S. MacPhee-BREA, unpublished data) and provided as a courtesy for use in the analyses presented here.

Genomics Approach

16S ribosomal (rRNA) marker gene surveys were conducted on freeze-dried sediments in order to assess the diversity and community structure of bacterial populations in the Beaufort Sea and Amundsen Gulf benthos. Sample preparation for sequencing had three steps: (1) total genomic

DNA was extracted from sediment samples using the Qiagen PowerSoil kit, (2) the V4 region of the 16S rRNA gene was amplified using revised forward and reverse primers from the Earth Microbiome Project (EMP) standard protocol, and (3) library preparation was completed with iTru adapters for sequencing. This last step was completed following the one-step polymerase chain reaction (PCR) protocol with indexed primers, which is the current standard protocol used by the EMP (Apprill et al., 2015; J. G. Caporaso et al., 2011; J. G. Caporaso et al., 2012; Parada, Needham, & Fuhrman, 2016; Walters et al., 2016). The processed samples were sequenced on the Illumina MiSeq platform in the DNA Core Laboratory facility at the University of Alaska Fairbanks (UAF).

DNA Sequence Processing

Once raw sequencing data were obtained, sequences were demultiplexed using the Mr. Demuxy package (Cock et al., 2009). To obtain a taxonomy table with operational taxonomic units (OTUs) for downstream analyses, sequences were run through the mothur toolkit on a high performance-computing cluster (through UAF Research Computing Systems) using a modified MiSeq standard operating procedure. OTUs were clustered at 99% similarity (see Appendix) (Schloss et al., 2009). Taxonomy was assigned to OTUs using the newest version of the SILVA reference database, SILVA 128 (Glöckner et al., 2017; Wang et al., 2007). The table comprising the relative abundance of OTUs identified for each sample was used to investigate the alpha-diversity (species richness) and beta-diversity (community structure) of bacterial assemblages from all 79 study sites and to assess correlations between environmental variables of these patterns. All analyses involving environmental data with OTU data were conducted with 77 of the 79 samples, as two samples did not have the associated environmental characteristics. Finally, a taxonomy table generated with mothur was searched for putative oil-degrading taxa to establish their presence or absence across all sample sites.

Statistical Analyses

All environmental variables were checked for normality using Q-Q plots and the Shapiro Wilkes test for normal distribution. Correlation between individual environmental variables was investigated using a combination of pairwise plots, linear regression models, and Spearman's Rho correlation coefficients in R (R Core Team, 2017). This was done to elucidate covarying environmental parameters. Alpha-diversity was investigated using the Inverse Simpson Index, which is generally preferable when trying to differentiate between multiple sites with varying environmental characteristics (Morris et al., 2014). Inverse Simpson indices were calculated using the vegan package in R (Oksanen et al., 2017; R Core Team, 2017). An nMDS plot using Bray-Curtis indices was constructed to visualize broad-scale patterns of overall bacterial community structure across the Beaufort Sea and the Amundsen Gulf. In order to accommodate such a large dataset, the OTU table was square root transformed and Wisconsin double-standardized, which is necessary to fit these data into 2-dimensional space with low-stress (< 0.15) (Link et al., 2013; Oksanen, 2015). Correlations between community structure and environmental variables were evaluated using the envfit function in the vegan R package to fit

environmental variables to nMDS plots with Bray-Curtis (Oksanen et al., 2017; R Core Team, 2017). Envfit calculates the vectors of environmental variables and fits these vectors to an nMDS ordination through QR decomposition, which is similar to linear regression, (Oksanen, 2015). The nMDS ordination constructed here is based on a distance matrix (Bray-Curtis); however, as long as the stress value of the nMDS ordination is low (< 0.15), the resulting linear representation of Bray-Curtis distances in nMDS space provides reasonable goodness of fit (R^2) values (Oksanen, 2015; Oksanen et al., 2017). Envfit also uses permutations to assess the significance of fitted vectors (i.e., environmental variables).

Results

Environmental Variables

The majority of environmental variables (80%) exhibited a non-normal distribution as indicated by Q-Q plots and significant values ($p<0.05$) yielded from the Shapiro-Wilkes tests for normality. These included depth, temperature, salinity, chl-*a*, phaeopigments, chl-*a*/ phaeopigments, $\delta^{13}C$, and C/N. A significant Shapiro-Wilkes p-value rejects the null of normally distributed data. Two variables, $\delta^{15}N$ and TOC, exhibited normal distributions. However, the Shapiro-Wilkes p-value for $\delta^{15}N$ was very close to significant ($p=0.053$; Table 1). Transformations appropriate to individual non-normal distributions were tested and applied. After transformation, many of the Q-Q plots exhibited normal distributions; however, many of the variables still failed the Shapiro-Wilkes test (i.e., transformed data exhibited closer to normal distributions but not necessarily normally distributed). For two of the environmental variables, salinity and $\delta^{13}C$, a transformation yielding a normal distribution could not be reached.

Table 1. Inherent characteristics of environmental variables**.** Normal distribution (ND), Potential outliers (PO), Transformation (Tf), Shapiro-Wilkes p-values before transformation (p-value) and after transformation (T p-values) NTf indicates that all transformations applied did not satisfy either the Q-Q plot or Shapiro-Wilkes test for normality, and N indicated normal distribution.

Environmental data	ND	PO	p-value	Tf	Tf p-value
Depth	No	0	6.1e-11	log	0.045
Salinity	No	0	3.1e-06	NTf	NTf
Temperature	No	1	2.2e-06	CBRT	3.9e-06
Chl-*a*	No	4	2.2e-16	log	0.048
Phaeopigment	No	3	6.4e-06	SQRT	0.22
Chl-*a* / Phaeopigment	No	4	2.2e-16	log	3.0e-07
δ15N*	Yes*	0	0.053	log	0.63
δ13C	No	9	6.5e-10	NTf	NTf
C/N	No	6	7.1e-06	log	0.014
TOC	Yes	2	0.1075	N	N

*A transformation for $\delta^{15}N$ was investigated due to the close to significant p=value prior to transformation.

Given the highly variable distributions of the environmental data explored here and the difficulty in achieving normal distribution through transformation for all variables, the downstream analyses herein are non-parametric. R^2 and p-values from linear regression models investigating correlations between environmental variables, with non-transformed and transformed data are presented in Appendix Table A2. These data may be useful for future parametric analyses such as principal components analysis (PCA) or canonical correspondence analysis (CCA).

Correlations between environmental variables were investigated using the Spearman's Rho (R_s) correlation coefficient. A visual representation of the R_s and p-values from correlation analyses is depicted in Figure 3. The strongest correlations exhibited among these environmental variables are between depth and salinity (R_s=0.94) and depth and chl-a/ phaeopigments (R_s= -0.76). There are a few moderate correlations (R_s=0.69–0.41) exhibited between variables and depth and salinity measures as well as between variables within the sediment pigments, isotopes, and organic matter characteristics (Figure 3). The remainder of correlation strengths are relatively low (R_s=0.39–0.02) and average to an R_s ~ 0.11. Appendix Table A3 provides a complete list of R_s and associated p-values.

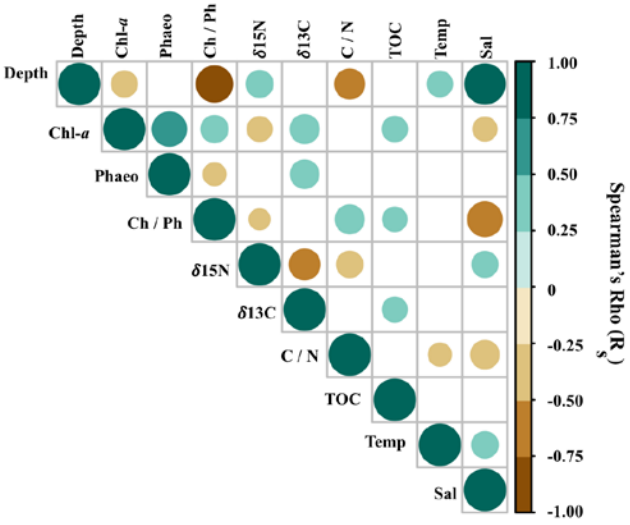

Figure 3. Correlations between environmental variables using Spearman's Rho. Empty grid-cells indicate correlations that were not significant (p>0.05). The presence of a sphere indicates a significant correlation (p<0.05) and size and color of the spheres illustrate the strength and nature (positive/negative) of the correlation, respectively.

Alpha-diversity

Inverse Simpson diversity indices calculated were organized in a bar plot form from west to east to investigate the overall trend in diversity across the study area (Figure 4). Bacterial diversity exhibits an increasing trend from west to east with mean inverse Simpson values of 236 for samples located west of the Mackenzie River and 298 for samples located east of the Mackenzie River. The mean Inverse Simpson value was 364 for the four samples collected directly north of the Mackenzie River.

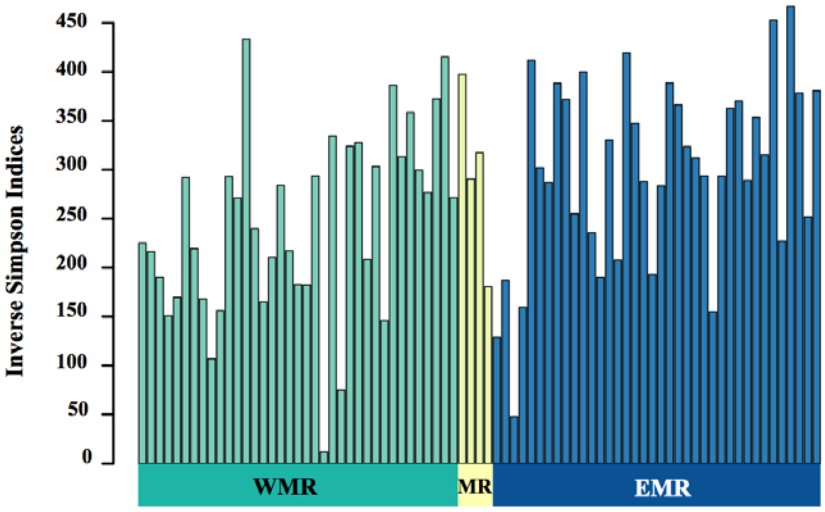

Figure 4. Diversity of bacteria from the Beaufort Sea to the Amundsen Gulf. The bar plot is organized on the x-axis from west to east. Samples are colored by their location relative to the Mackenzie River (MR) (west=WMR and east=EMR), which is a natural and influential divide in the study area.

Spearman's Rho was used to investigate correlations between environmental variables and diversity (Figure 5). The overall correlation strengths between diversity and environmental variables are moderate (R_s=0.5~0.4) to low (R_s<0.4). Diversity is correlated most strongly with salinity, depth (positive), and chl-*a* (negative).

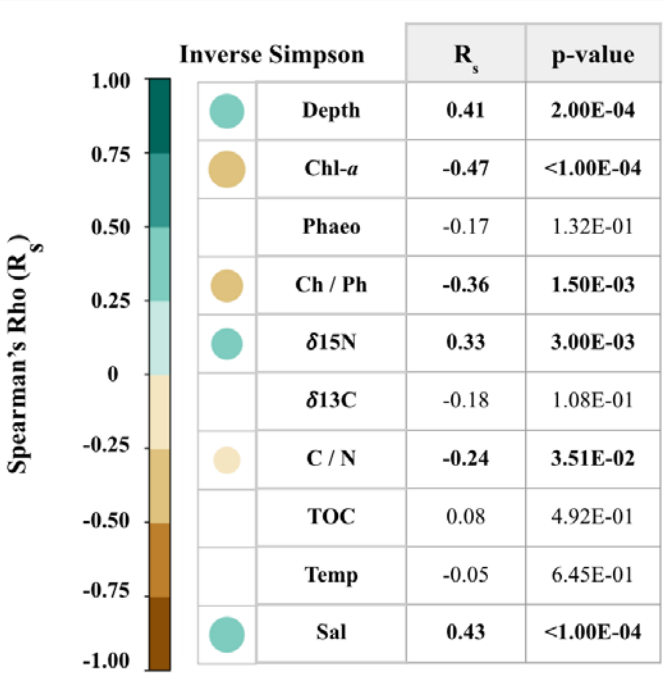

Inverse Simpson	R_s	p-value
Depth	**0.41**	**2.00E-04**
Chl-*a*	**-0.47**	**<1.00E-04**
Phaeo	-0.17	1.32E-01
Ch / Ph	**-0.36**	**1.50E-03**
δ15N	**0.33**	**3.00E-03**
δ13C	-0.18	1.08E-01
C / N	**-0.24**	**3.51E-02**
TOC	0.08	4.92E-01
Temp	-0.05	6.45E-01
Sal	**0.43**	**<1.00E-04**

Figure 5. Correlations between diversity and environmental variables**.** Empty grid-cells indicate correlations that were not significant (p>0.05). The presence of a sphere and bold text indicates a significant correlation (p<0.05), sphere size and color illustrate the strength and nature (positive/negative) of the correlation, respectively.

Beta-diversity

Loose clustering and overall nMDS plot distribution indicate that there are inherent dissimilarities in bacterial community structure; however, but grouping variables are more difficult to discern (Figure 6). In spite of a large amount of overlap, clustering of Alaskan Beaufort Shelf communities appears on the lower portion of the nMDS and of Mackenzie Shelf communities on the upper portion of the nMDS. Except for one sample, the Banks Island samples cluster together. The Amundsen Gulf communities are distributed more sporadically. A PERMANOVA indicates that the bacterial communities between these regions are significantly different (p=0.001) but with a low R^2 (0.1). The variable 'year' was also investigated using a PERMANOVA and showed no significant effect on bacterial community structure.

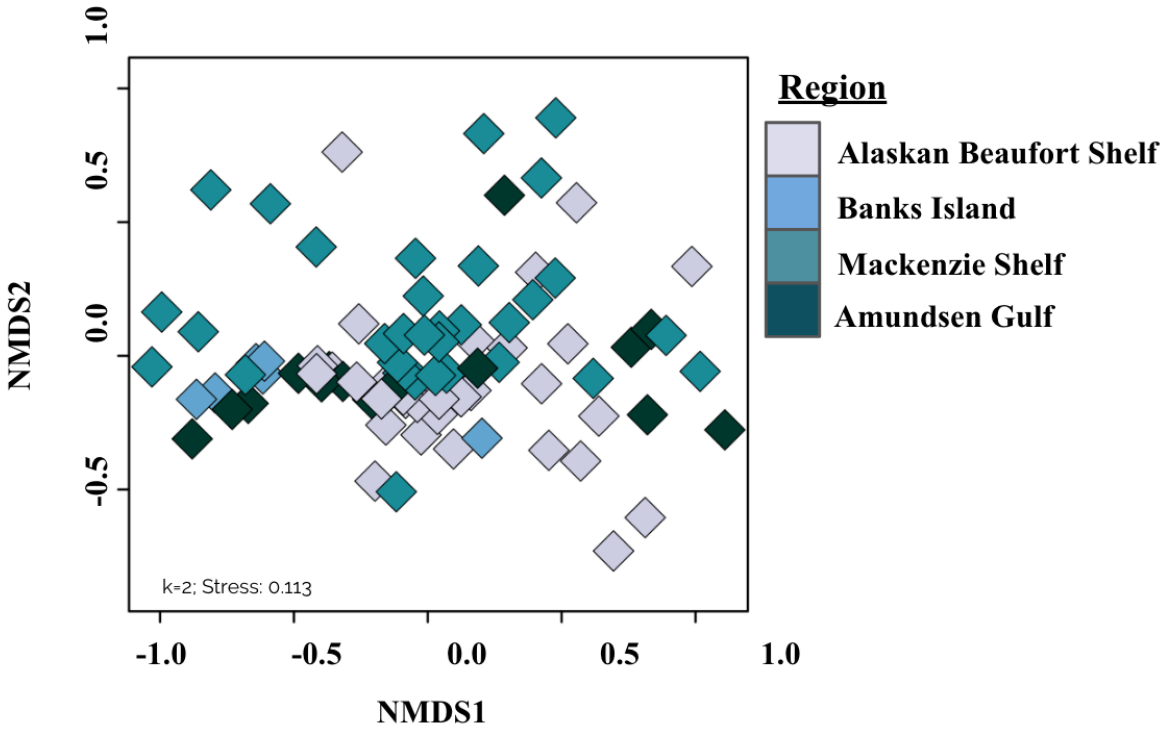

Figure 6. Bacterial community structure across the Beaufort Sea and the Amundsen Gulf in nMDS ordination space colored by region

Environmental Correlations

Potential environmental drivers of community structure were examined using the envfit function in the R package vegan (Oksanen et al., 2017). The best results from envfit are produced when the nMDS ordination to be fitted exhibits low stress. According to Clarke, stress value designations are as follows: >0.20=unacceptable, <0.20=acceptable, <0.10=good, and <0.05=ideal (Clarke, 1988). The nMDS ordination depicted in Figure 6 only has acceptable stress (0.11) in 2-D space (k=2). Therefore, to ensure more accurate vector fitting and R^2 values and associated p-values, environmental variables were fitted with an nMDS in 3-D space (k=3), which has good stress (0.07). R^2 and p-values from applying envfit with 999 permutations to the

nMDS ordination (bacterial community structure) and fitted environmental variables are listed in Table 2. Depth, chl-*a*, $\delta^{15}N$, C/N, TOC, and salinity are significantly correlated, i.e., explain some portion (R^2) of the variation in bacterial community structure across the Beaufort Sea and Amundsen Gulf benthos. Variables that are significantly ($p<0.05$) correlated with bacterial community structure explain relatively low percentages of variance (10–42%). The output from envfit, nMDS axes, and associated R^2 and p-values were plotted with the nMDS ordination with the lowest stress (Figure 7). This plot indicates that the significant correlates of bacterial community structure are not equally affecting all samples in the study area. Depth, salinity, and $\delta^{15}N$ have maximum correlations with samples on the left side of the nMDS, while chl-*a*, C/N, and TOC exhibited maximum correlations with samples on the right side of the nMDS.

Table 2. Correlations between environmental variables and bacterial community structure. Significant correlation values are bold.

Environmental Drivers	envfit() R^2	envfit() Pr(>r)
Depth	**0.3132**	**0.001**
Chl-*a*	**0.1687**	**0.001**
Phaeopigment	0.0379	0.261
Chl-*a* / Phaeopigment	0.0619	0.136
δ15N	**0.3405**	**0.001**
δ13C	0.0156	0.562
C/N	**0.1846**	**0.001**
TOC	**0.1045**	**0.013**
Temperature	0.0619	0.136
Salinity	**0.4278**	**0.001**

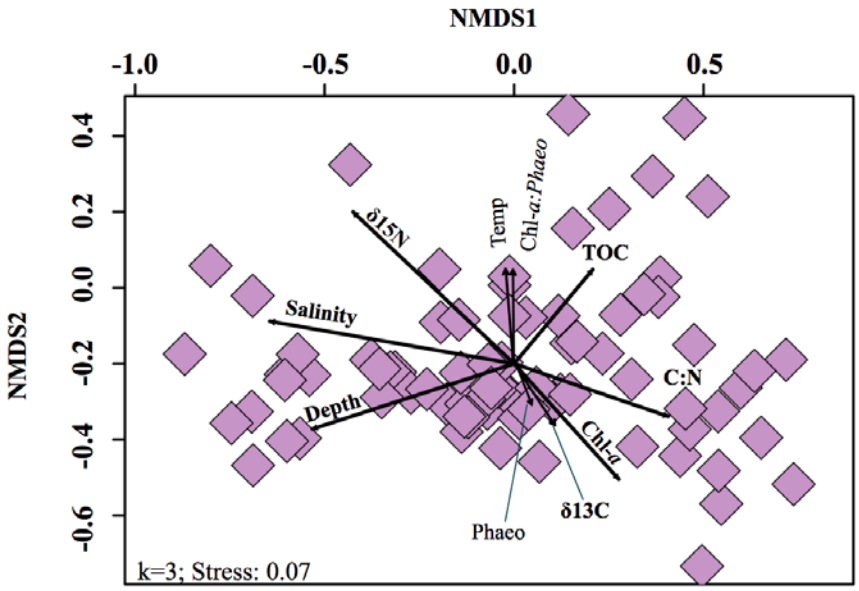

Figure 7. Correlation between environmental variables and bacterial community structure in nMDS ordination space with fitted vectors. Environmental vectors that are stronger predictors have longer arrows than weaker predictors. Arrow directions indicate the area (refer to Figure 6) in which the environmental vectors have maximum correlations and change most rapidly in ordination space (Oksanen et al., 2017)

Putative Oil-degraders

All of the potential oil-degrading taxa, except *Microbulbifer*, were present in low relative abundances within the study area (Figure 8). *Alcanivoracaceae*, *Colwellia*, and *Shewanella* were present at a majority of the 77 sights.

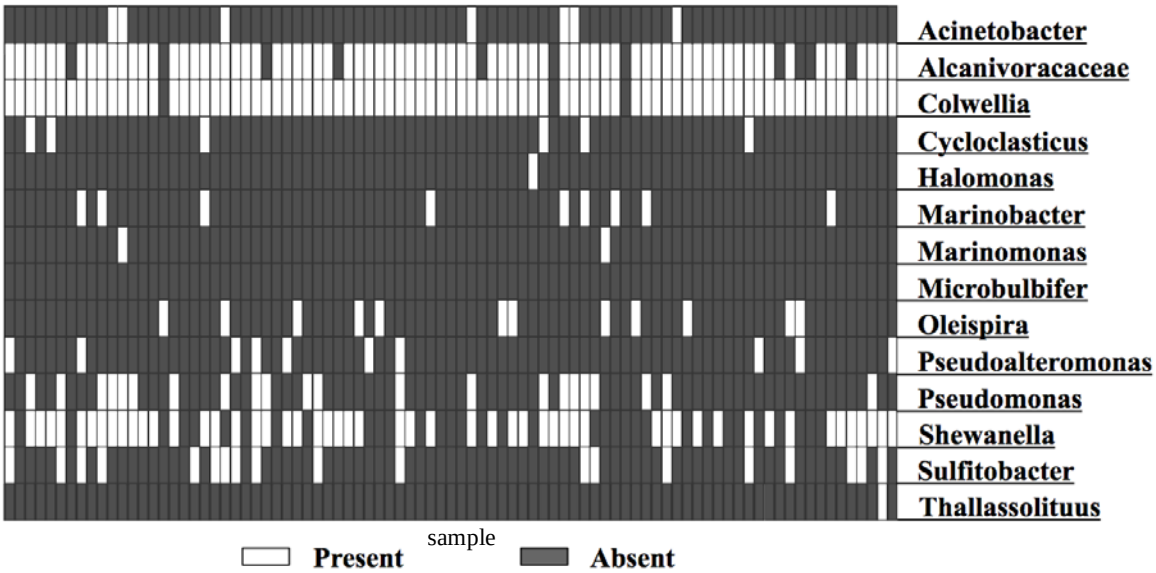

Figure 8. Putative oil-degrading taxa found in Beaufort Sea sediments. Each verticle stack of 14 blocks represents one sample.

Discussion

The goals of this study were to identify large-scale patterns of bacterial diversity and community structure and to identify environmental correlates of community structure in a highly dynamic sector of the Arctic. This sector, from the western Beaufort Sea to the Amundsen Gulf, encompasses a vast array of varying oceanographic characteristics including bathymetry, hydrology, terrigenous input, and annual sea ice dynamics. The majority of oceanographic and biological studies from this sector in the Arctic are region-specific (i.e., the Alaskan Beaufort Shelf, the Mackenzie Shelf, and the Amundsen Gulf), in part, due to the distinct oceanographic qualities that characterize each of these regions. In light of this, results from this study are interpreted using both broad-scale patterns for the entire study area and regional patterns reported in the literature.

The presence of depth-associated water masses is a broad-scale characteristic of this Arctic sector. In general, a fresher Polar Mixed layer is found from ~0–50 m, a Pacific layer from ~50–200 m, and a warmer, more saline Atlantic layer at depths greater than 200 m (Lansard et al., 2012; Miquel et al., 2015; Smoot & Hopcroft, 2017). Salinity and temperature characteristics demarcate the depth-distribution of these water masses. It is likely that patterns of bacterial diversity and community structure reflect these characteristics as benthic bacterial diversity significantly increases with depth (R_s=0.41) and salinity (R_s=0.43) across the Beaufort Sea and the Amundsen Gulf. Additionally, bacterial community structure is significantly correlated with depth and salinity. Although depth and salinity are highly correlated (R_s=0.94), similar and even higher R-values of salinity over depth may indicate that both influence bacterial communities. Hamdan et al. (2013) found water masses, and salinity, in particular, to be a driving force in benthic bacterial and archaeal communities from Alaskan Beaufort Shelf sediments (Hamdan et al., 2013). Studies characterizing benthic macro-organisms from the Mackenzie Shelf to the Amundsen Gulf also found salinity to be significantly correlated with community structure (Cusson, Archambault, & Aitken, 2007; Darnis et al., 2012).

Sediment $\delta^{15}N$, which is also positively correlated with depth and salinity (R_s~0.4), is significantly correlated with bacterial diversity (R_s=0.33) and community structure. Bulk $\delta^{15}N$ sediment values generally increase with water depth and can be used as a proxy for alteration of nitrogenous compounds throughout the water column and in the benthos. It is not surprising that $\delta^{15}N$ and bacterial community structure and diversity are significantly linked because bacteria and archaea dominate nitrogen-related processes in marine sediments and are capable of denitrification, nitrification, nitrogen fixation, and annamox (Devol, 2015). The significant correlation between bacteria and $\delta^{15}N$ highlights the importance of $\delta^{15}N$ as a proxy over $\delta^{13}C$ with respect to sediment bacteria on the scale of this study. This theory is supported by the lack of a significant correlation between $\delta^{13}C$ and bacterial diversity or community structure. However, $\delta^{13}C$ data exhibit a bimodal or even trimodal distribution, which may interfere with identifying it as a significant correlate in an area with such a large range of $\delta^{13}C$ values.

$\delta^{13}C$ was not significantly correlated with bacterial communities, but C/N and TOC were

correlated. C/N is negatively correlated with bacterial diversity and significantly correlated with bacterial community structure. C/N reflects the degree of degradation that has occurred in organic matter and may be affected by similar processes that influence the $\delta^{15}N$ of sediments, leading both variables to be significantly correlated with bacterial community structure. This is further supported by the relationship between C/N and diversity being negative. TOC is not significantly correlated with bacterial diversity but is significantly correlated with community structure. These findings, with respect to carbon, indicate that the source is not as important as the amount of carbon present in structuring bacterial communities. The “freshness" of organic carbon is also a potential driver in structuring bacterial communities, as there is a significant correlation between bacterial diversity and community structure with chl-*a*. Chl-*a* is negatively correlated with bacterial biodiversity. Chl-*a*/phaeopigments are also negatively correlated with bacterial diversity but are not significantly correlated to bacterial community structure. The findings with respect to correlations between diversity and sediment pigments are in contrast to findings reported from the Laptev Sea shelf edge and slope (Eurasian Arctic), which showed significant increases in bacterial diversity with increasing chl-*a* and phaeopigments (Bienhold et al., 2012b).

An investigation of contaminant degradation potential is relevant because the study area is located in an environment where both natural gas/oil seeps and anthropogenic resource exploration occur. To that end, the presence and absence of putative oil-degrading taxa were investigated across all sediment samples. Contaminant degradation studies have shown that increased diversity of bacteria is linked to higher degradation potential of contaminants *in situ* and in the laboratory (e.g., Head et al., 2006; Röling et al., 2002). In addition, a study looking at how natural and anthropogenic oil exposure affects diversity found that small amounts of oil (natural levels) were correlated with increased diversity while increasing oil concentrations, as might be associated with an exposure event, corresponded in a decrease in bacterial diversity (Orcutt et al., 2010), likely due to enrichment of oil-degrading taxa.

The presence of putative oil-degrading taxa, coupled with diversity estimates, indicates a capacity of oil biodegradation exists in these sediments. Putative oil-degrading bacteria generally occur naturally in the marine system and are more prevalent in areas exposed to natural or anthropogenic inputs of oil and petroleum product. The putative oil-degrading bacteria investigated here comprised a list of 13 genera and one family that have been identified through oil degradation studies in Arctic seawater (McFarlin et al., 2014; Prince et al., 2013). These taxa are not definitively linked with oil degradation but are capable of multiple modes of metabolism. They are implicated as playing a role in oil degradation because they have been found to increase significantly in relative abundance following oil exposure. Three taxa exhibited an almost ubiquitous distribution across the region: *Alcanivoracaceae, Colwellia,* and *Shewanella*. Members of the *Alcanivoracaceae* family are widespread in marine environments and include species that are directly linked to oil biodegradation (Silveira & Thompson, 2014). *Colwellia* are also commonly found in marine environments, though many of the species within this genus are psychrophilic and found more commonly in polar regions (Bowman et al., 1998). The genus

Shewanella is commonly found in low temperature and high-pressure (deeper) marine systems. This genus is highly metabolically versatile and has been identified in the biodegradation of heavy metals, such as iron and uranium, in addition to oil (Tiedje, 2002). *Microbulbifer* was the only taxa absent from all sites. The remaining ten taxa were sporadically distributed with more taxa present on the Alaska Beaufort Shelf and the Amundsen Gulf than on the Mackenzie Shelf.

This overview of the broad-scale patterns exhibited by benthic bacteria from the western Beaufort Sea to the Amundsen Gulf provides a solid foundation for additional analyses, with this and similar datasets, and can inform future field and laboratory research. Additional investigation of the environmental variables presented here, by region (i.e., the Alaskan Beaufort Shelf, Mackenzie Shelf, and the Amundsen Gulf), would provide insight into the processes shaping bacterial communities on a regional scale. Furthermore, this study highlights the need to explore additional environmental correlates of bacterial communities in Arctic sediments.

Acknowledgments

I would like to sincerely thank CMI and BOEM for providing students with the opportunity to follow their research passions and participate as principal investigators. A huge thank you to my advisors Dr. Sarah Hardy and Dr. Mary Beth Leigh for all of their help and guidance throughout this process and for the matched funding that they provided. I would like to extend my gratitude to Dr. Eric Collins and the UAF Research Computing Systems for providing me with matching funds, valuable assistance, and a platform on which to analyze my data. This work was supported in part by the high-performance computing and data storage resources operated by the Research Computing Systems Group at the University of Alaska Fairbanks, Geophysical Institute and BOEM under (M16AC00004).

References

Apprill, A., McNally, S., Parsons, R., & Weber, L. (2015). Minor revision to V4 region SSU rRNA 806R gene primer greatly increases detection of SAR11 bacterioplankton. Aquatic Microbial Ecology, 75(2), 129–137. doi.org/10.3354/ame01753

Arndt, S., Jørgensen, B. B., Larowe, D. E., Middelburg, J. J., Pancost, R. D., & Regnier, P. (2013). Earth-Science Reviews Quantifying the degradation of organic matter in marine sediments: A review and synthesis. Earth Science Reviews, 123, 53–86. doi.org/10.1016/j.earscirev.2013.02.008

Bienhold, C., Boetius, A., & Ramette, A. (2012a). The energy-diversity relationship of complex bacterial communities in Arctic deep-sea sediments. The ISME Journal, 6(4), 724–32. doi.org/10.1038/ismej.2011.140

Bienhold, C., Boetius, A., & Ramette, A. (2012b). The energy–diversity relationship of complex bacterial communities in Arctic deep-sea sediments. The ISME Journal, 6(4), 724–732. doi.org/10.1038/ismej.2011.140

Bowman, J. P., Gosink, J. J., McCammon, S. A., Lewis, T. E., Nichols, D. S., Nichols, P. D., Skerratt, J. H., Staley, J. T., & McMeekin, T. A. (1998). *Colwellia demingiae* sp. nov., *Colwellia hornerae* sp. nov., *Colwellia rossensis* sp. nov. and *Colwellia psychrotropica* sp. nov.: psychrophilic Antarctic species with the ability to synthesize docosahexaenoic acid. International Journal of Systematic Bacteriology, 48(4), 1171–1180. doi.org/10.1099/00207713-48-4-1171

Bureau of Ocean Energy Management (BOEM). (2012). Arctic Ocean Oil and Gas Lease Planning. Retrieved October 2017 from http://www.arcgis.com/home/item.html?id=ec25cf340e8b42bda6cb03c9aa512c8a

Buttigieg, P. L., & Ramette, A. (2015). Biogeographic patterns of bacterial microdiversity in Arctic deep-sea sediments (HAUSGARTEN, Fram Strait). Frontiers in Microbiology, 5:660. doi.org/10.3389/fmicb.2014.00660

Conservation of Arctic Flora and Fauna/United States Geological Survey (CAFF/USGS). (2017). Circumpolar distribution and probability of potential petroleum reserves in the North. Retrieved August 11, 2017, from http://geo.abds.is/geonetwork/srv/eng/catalog.search#/metadata/8b1233d0-96cb-476b-a8c6-7c3609f7e8a5

Caporaso, J. G., Lauber, C. L., Walters, W. A., Berg-Lyons, D., Lozupone, C. A., Turnbaugh, P. J., Fierer, N., & Knight, R. (2011). Global patterns of 16S rRNA diversity at a depth of millions of sequences per sample. Proceedings of the National Academy of Sciences, 108(Supplement_1), 4516–4522. doi.org/10.1073/pnas.1000080107

Caporaso, J. G., Lauber, C. L., Walters, W. A , Berg-Lyons, D., Huntley, J., Fierer, N., Owens, S. M., Betley, J., Fraser, L., Bauer, M., Gormley, N. Gilbert, J. A., Smith, G., & Knight, R. (2012). Ultra-high-throughput microbial community analysis on the Illumina HiSeq and MiSeq platforms. The ISME Journal, 6(8), 1621–1624. doi.org/10.1038/ismej.2012.8

Carmack, E. C., & Macdonald, R. W. (2002). Oceanography of the Canadian Shelf of the Beaufort Sea: A Setting for Marine Life. Arctic, 55(5), 29–45. doi.org/10.14430/arctic733

Clarke, K. R. (1988). Non-parametric multivariate analyses of changes in community structure. Australian Journal of Ecology, 18(1988), 117–143. doi.org/10.1111/j.1442-9993.1993.tb00438.x

Cock, P. J. A., Antao, T., Chang, J. T., Chapman, B. A., Cox, C. J., Dalke, A., Friedberg, I., Hamelryck, T., Kauff, F., Wilczynski, B., & de Hoon, M. J. L. (2009). Biopython: freely available Python tools for computational molecular biology and bioinformatics. Bioinformatics, 25(11), 1422–1423. doi.org/10.1093/bioinformatics/btp163

Cusson, M., Archambault, P., & Aitken, A. (2007). Diversity of benthic assemblages on the Arctic continental shelf: Historical data from Canada. Marine Ecology Progress Series, 331, 291–304. doi.org/10.3354/meps331291

Darnis, G., Robert, D., Pomerleau, C., Link, H., Archambault, P., Nelson, R. J., Geoffroy, M., Tremblay J.-E., Lovejoy, C., Ferguson, S. H., Hunt, B. P. V., & Fortier, L. (2012). Current state and trends in Canadian Arctic marine ecosystems: II. Heterotrophic food web, pelagic-benthic coupling, and diversity. Climatic Change, 115(1), 179–205. doi.org/10.1007/s10584-012-0483-8

Dell'Anno, A., Beolchini, F., Rocchetti, L., Luna, G. M., & Danovaro, R. (2012). High bacterial diversity increases degradation performance of hydrocarbons during bioremediation of contaminated harbor marine sediments. Environmental Pollution, 167, 85–92. doi.org/10.1016/j.envpol.2012.03.043

Deming, J. W., & Baross, J. A. (1993). The early diagenesis of organic matter: bacterial activity. In Engel, M. & Mackel, S. (eds.), Organic Geochemistry. Plenum Press, New York.

Devol, A. H. (2015). Denitrification, Anammox, and N_2 Production in Marine Sediments. Annual Review of Marine Science, 7(1), 403–423. doi.org/10.1146/annurev-marine-010213-135040

Dunton, K. H., Weingartner, T., & Carmack, E. C. (2006). The nearshore western Beaufort Sea ecosystem: Circulation and importance of terrestrial carbon in arctic coastal food webs. Progress in Oceanography, 71, 362–378. doi.org/10.1016/j.pocean.2006.09.011

Forest, A., Bélanger, S., Sampei, M., Sasaki, H., Lalande, C., & Fortier, L. (2010). Three-year assessment of particulate organic carbon fluxes in Amundsen Gulf (Beaufort Sea): Satellite observations and sediment trap measurements. Deep-Sea Research Part I: Oceanographic Research Papers, 57(1), 125–142. doi.org/10.1016/j.dsr.2009.10.002

Fuhrman, J. A. (2009). Microbial community structure and its functional implications. Nature, 459(7244), 193–199. doi.org/10.1038/nature08058

Gamboa, A., Montero-Serrano, J.-C., St-Onge, G., Rochon, A., & Desiage, P.-A. (2017). Mineralogical, geochemical, and magnetic signatures of surface sediments from the Canadian Beaufort Shelf and Amundsen Gulf (Canadian Arctic). Geochemistry, Geophysics, Geosystems, 18(2), 488–512. doi.org/10.1002/2016GC006477

Glöckner, F. O., Yilmaz, P., Quast, C., Gerken, J., Beccati, A., Ciuprina, A., Bruns, G., Yarza, P., Peplies, J., Westram, R., & Ludwig, W. (2017). 25 years of serving the community with ribosomal RNA gene reference databases and tools. Journal of Biotechnology, 261, 169–176. doi.org/10.1016/j.jbiotec.2017.06.1198

Hamdan, L. J., Coffin, R. B., Sikaroodi, M., Greinert, J., Treude, T., & Gillevet, P. M. (2013). Ocean currents shape the microbiome of Arctic marine sediments. The ISME Journal, 7(4), 685–696. doi.org/10.1038/ismej.2012.143

Head, I. M., Jones, D. M., & Röling, W. F. M. (2006). Marine microorganisms make a meal of oil. Nature Reviews Microbiology, 4(3), 173–182. doi.org/10.1038/nrmicro1348

Jacob, M., Soltwedel, T., Boetius, A., & Ramette, A. (2013). Biogeography of Deep-sea benthic bacteria at a regional scale (LTER HAUSGARTEN, Fram Strait, Arctic). PLoS ONE, 8(9), e72779. doi.org/10.1371/journal.pone.0072779

Judd, K. E., Crump, B. C., & Kling, G. W. (2006). Variation in dissolved organic matter controls bacterial production and community composition. Ecology, 87(8), 2068–2079. doi.org/10.1890/0012-9658(2006)87[2068:VIDOMC]2.0.CO;2

Lansard, B., Mucci, A., Miller, L. A., Macdonald, R. W., & Gratton, Y. (2012). Seasonal variability of water mass distribution in the southeastern Beaufort Sea determined by total alkalinity and $\delta^{18}O$. Journal of Geophysical Research: Oceans, 117, C03003. doi.org/10.1029/2011JC007299

Link, H., Chaillou, G., Forest, A., Piepenburg, D., & Archambault, P. (2013). Multivariate benthic ecosystem functioning in the Arctic-benthic fluxes explained by environmental parameters in the southeastern Beaufort Sea. Biogeosciences, 10, 5911–5929. doi.org/10.5194/bg-10-5911-2013

Lopez, G. R., & Levinton, J. S. (1987). Ecology of deposit-feeding animals in marine sediments. The Quarterly Review of Biology, 62(3), 235–260.

Magen, C., Chaillou, G., Crowe, S. A., Mucci, A., Sundby, B., Gao, A., Macabe, R., & Sasaki, H. (2010). Origin and fate of particulate organic matter in the southern Beaufort Sea - Amundsen Gulf region, Canadian Arctic. Estuarine, Coastal and Shelf Science, 86(1), 31–41. doi.org/10.1016/j.ecss.2009.09.009

McFarlin, K. M., Prince, R. C., Perkins, R., & Leigh, M. B. (2014). Biodegradation of dispersed oil in Arctic seawater at -1°C. PLoS ONE, 9(1), 1–8. doi.org/10.1371/journal.pone.0084297

McKew, B. A., Coulon, F., Osborn, A. M., Timmis, K. N., & McGenity, T. J. (2007). Determining the identity and roles of oil-metabolizing marine bacteria from the Thames estuary, UK. Environmental Microbiology, 9(1), 165–176.

Mincks, S. (2005). Persistence of labile organic matter and microbial biomass in Antarctic shelf sediments: evidence of a sediment food bank. Marine Ecology Progress Series, 300, 3–19. doi.org/10.2307/24869726

Miquel, J. C., Gasser, B., Martín, J., Marec, C., Babin, M., Fortier, L., & Forest, A. (2015). Downward particle flux and carbon export in the Beaufort Sea, Arctic Ocean; the role of zooplankton. Biogeosciences, 12(16), 5103–5117. doi.org/10.5194/bg-12-5103-2015

Morris, D. J., O'Connell, M. T., & Macko, S. A. (2015). Assessing the importance of terrestrial organic carbon in the Chukchi and Beaufort Seas. Estuarine, Coastal and Shelf Science, 164, 28–38. doi.org/10.1016/j.ecss.2015.06.011

Morris, E. K., Caruso, T., Buscot, F., Fischer, M., Hancock, C., Maier, T. S., Meiners, T., Müller, C., Obermaier, E., Prati, D., Socher, S. A., Sonnemann, I.,Wäschke, N., Wubet, T., Wurst, S., & Rillig, M. C. (2014). Choosing and using diversity indices: insights for ecological applications from the German Diversity Exploratories. Ecology and Evolution, 4(18), 3514–3524. doi.org/10.1002/ece3.1155

Oksanen, J. (2015). Multivariate Analysis of Ecological Communities in R: vegan tutorial. Retrieved from http://cc.oulu.fi/~jarioksa/opetus/metodi/vegantutor.pdf

Oksanen, J., Blanchet, F. G., Friendly, M., Kindt, R., Legendre, P., Mcglinn, D., & Oksanen, M. J. (2017). Title Community Ecology Package. Retrieved from https://github.com/vegandevs/vegan/issues

Orcutt, B. N., Joye, S. B., Kleindienst, S., Knittel, K., Ramette, A., Reitz, A., Samarkin, V., Treude, T., & Boetius, A. (2010). Impact of natural oil and higher hydrocarbons on microbial diversity, distribution, and activity in Gulf of Mexico cold-seep sediments. Deep-Sea Research Part II: Topical Studies in Oceanography, 57(21), 2008–2021. doi.org/10.1016/j.dsr2.2010.05.014

Ortega-Retuerta, E., Joux, F., Jeffrey, W. H., & Ghiglione, J. F. (2013). Spatial variability of particle-attached and free-living bacterial diversity in surface waters from the Mackenzie River to the Beaufort Sea (Canadian Arctic). Biogeosciences, 10, 2747–2759. doi.org/10.5194/bg-10-2747-2013

Parada, A. E., Needham, D. M., & Fuhrman, J. A. (2016). Every base matters: assessing small subunit rRNA primers for marine microbiomes with mock communities, time series and global field samples. Environmental Microbiology, 18(5), 1403–1414. doi.org/10.1111/1462-2920.13023

Pickart, R. S. (2004). Shelfbreak circulation in the Alaskan Beaufort Sea: Mean structure and variability. Journal of Geophysical Research C: Oceans, 109(4), 1–14. doi.org/10.1029/2003JC001912

Prince, R. C., McFarlin, K. M., Butler, J. D., Febbo, E. J., Wang, F. C. Y., & Nedwed, T. J. (2013). The primary biodegradation of dispersed crude oil in the sea. Chemosphere, 90(2), 521–526. doi.org/10.1016/j.chemosphere.2012.08.020

Rachold, V., Eicken, H., Gordeev, V. V, Grigoriev, M. N., & Hubberten, H. (2004). The Organic Carbon Cycle in the Arctic Ocean. doi.org/10.1007/978-3-642-18912-8

R Core Team. (2017). R: A language and environment for statistical computing. Vienna, Austria: R Foundation for Statistical Computing. Retrieved from https://www.r-project.org/

Robinson, R. S., Kienast, M., Albuquerque, A., Altabet, M., Contreras, S., De Pol Holz, R., & Yang, J. -Y. (2012). A review of nitrogen isotopic alteration in marine sediments. Paleoceanography, 27(4). doi.org/10.1029/2012PA002321

Röling, W. F. M., Milner, M. G., Jones, D. M., Lee, K., Daniel, F., Swannell, R. J. P., & Head, I. M. (2002). Robust hydrocarbon degradation and dynamics of bacterial communities during nutrient-enhanced oil spill bioremediation. Applied and Environmental Microbiology, 68(11), 5537–5548.

Schloss, P. D., Westcott, S. L., Ryabin, T., Hall, J. R., Hartmann, M., Hollister, E. B.,Lesniewski, R. A., Brian B. Oakley, B. B., Parks, D., Robinson, C. J., Sahl, J. W., Stres, B., Thallinger, G., Van Horn, D. J., & Weber, C. F. (2009). Introducing mothur: Open-source, platform-independent, community-supported software for describing and comparing microbial communities. Applied and Environmental Microbiology, 75(23), 7537–7541. doi.org/10.1128/AEM.01541-09

Silveira, C. B., & Thompson, F. (2014). The Family *Alcanivoraceae*. In: Rosenberg, E., DeLong, E.F., Lory, S., Stackebrandt, E., & Thompson, F. (eds), The Prokaryotes. Springer, Berlin, Heidelberg. doi.org/10.1007/978-3-642-38922-1_369

Smoot, C. A., & Hopcroft, R. R. (2017). Depth-stratified community structure of Beaufort Sea slope zooplankton and its relations to water masses. Journal of Plankton Research, 39(1), 79–91. doi.org/10.1093/plankt/fbw087

Stokes, C. R., Clark, C. D., & Winsborrow, M. C. M. (2006). Subglacial bedform evidence for a major palaeo-ice stream and its retreat phases in Amundsen Gulf, Canadian Arctic Archipelago. Journal of Quaternary Science, 21(4), 399–412. doi.org/10.1002/jqs.991

Tesdal, J.-E., Galbraith, E. D., & Kienast, M. (2013). Nitrogen isotopes in bulk marine sediment: linking seafloor observations with subseafloor records. Biogeosciences, 10(1), 101–118. doi.org/10.5194/bg-10-101-2013

Teske, A., Durbin, A., Ziervogel, K., Cox, C., & Arnosti, C. (2011). Microbial community composition and function in permanently cold seawater and sediments from an Arctic fjord of Svalbard. Applied and Environmental Microbiology, 77(6), 2008–2018. doi.org/10.1128/AEM.01507-10

Tiedje, J. M. (2002). *Shewanella*—the environmentally versatile genome. Nature Biotechnology, 20(11), 1093–1094. doi.org/10.1038/nbt1102-1093

Walters, W., Hyde, E. R., Berg-Lyons, D., Ackermann, G., Humphrey, G., Parada, A., & Knight, R. (2016). Improved bacterial 16S rRNA gene (V4 and V4-5) and fungal internal transcribed spacer marker gene primers for microbial community surveys. mSystems, 1(1), e00009-15. doi.org/10.1128/mSystems.00009-15

Wang, Q., Garrity, G. M., Tiedje, J. M., & Cole, J. R. (2007). Naive Bayesian classifier for rapid assignment of rRNA sequences into the new bacterial taxonomy. Applied and Environmental Microbiology, 73(16), 5261–5267. doi.org/10.1128/AEM.00062-07

Yakimov, M. M., Timmis, K. N., & Golyshin, P. N. (2007). Obligate oil-degrading marine bacteria. Current Opinion in Biotechnology, 18(3), 257–266. doi.org/10.1016/j.copbio.2007.04.006

Zinger, L., Amaral-Zettler, L. A., Fuhrman, J. A., Horner-Devine, M. C., Huse, S. M., Welch, D. B. M., Martiny, J. B. H., Sogin, M., Boetius, A., & Ramette, A. (2011). Global patterns of bacterial beta-diversity in seafloor and seawater ecosystems. PLoS ONE, 6(9), 1–11. doi.org/10.1371/journal.pone.0024570

Appendices

Table A1. Collection information for all sediment samples.

Sample	Latitude	Longitude	Year	Cruise	Depth (m)
B2.50A	71.167	-151.100	2012	USTB	50
B1.200A	71.230	-150.084	2012	USTB	200
B1.200B	71.230	-150.084	2012	USTB	200
B1.200C	71.230	-150.084	2012	USTB	200
B1.500B	71.250	-150.084	2012	USTB	500
B1.1000	71.283	-150.084	2012	USTB	1000
A6.37	70.451	-146.102	2014	USTB	37
A6.20	70.274	-146.093	2014	USTB	20
A5.35	70.334	-145.110	2014	USTB	35
A5.20	70.119	-145.107	2014	USTB	20
A5.50	70.547	-145.081	2014	USTB	51
A5.100	70.715	-145.075	2014	USTB	101
A5.350	70.840	-145.062	2014	USTB	350
A4.100	70.582	-144.153	2014	USTB	107
A4.20	70.201	-144.100	2014	USTB	20
A4.50	70.462	-144.082	2014	USTB	54
A4.35	70.290	-144.072	2014	USTB	37
A2.20	69.979	-142.216	2014	USTB	21.6
A2.50	70.303	-142.139	2014	USTB	52.5
A2.350	70.540	-142.077	2014	USTB	349
A2.100	70.476	-141.926	2014	USTB	109
A2.200	70.497	-141.902	2014	USTB	200
A1.200	70.366	-141.152	2014	USTB	201
A1.20	69.719	-141.139	2014	USTB	20
A1.02	70.333	-141.117	2013	BREA	75
A1.100	70.333	-141.058	2014	USTB	99
A1.04	70.400	-141.050	2013	BREA	350
A1.350	70.406	-141.034	2014	USTB	350
A1.50	70.031	-141.032	2014	USTB	50
A1.06	70.533	-141.017	2013	BREA	750
TBS.350	70.342	-140.391	2014	USTB	347
TBS.04	70.334	-140.367	2013	BREA	350
TBS.200	70.270	-140.306	2014	USTB	203
TBS.100	70.246	-140.303	2014	USTB	101
GRY.06	70.433	-138.983	2013	BREA	750
GRY.04	70.250	-138.367	2013	BREA	350
DWT.01	70.584	-138.317	2013	BREA	1200
GRY.02	70.000	-137.667	2013	BREA	75
KUG.04	70.977	-134.786	2014	BREA	327
KUG.03	70.932	-134.745	2014	BREA	201

Sample	Latitude	Longitude	Year	Cruise	Depth (m)
KUG.02	70.849	-134.668	2014	BREA	77.8
KUG.01	70.009	-133.844	2014	BREA	20.5
AGK.02	70.047	-133.560	2014	BREA	29.5
ESC.04	70.088	-132.139	2014	BREA	19
ESC.03	70.338	-131.005	2014	BREA	17
BNK.03	72.092	-129.974	2014	BREA	364
BNK.04	72.099	-128.817	2014	BREA	379
BNK.05	72.928	-127.791	2014	BREA	252
BNK.02	72.098	-127.481	2014	BREA	350
BNK.07	72.101	-127.143	2014	BREA	192
FRK.07	70.088	-126.919	2014	BREA	37
NTC.01	71.314	-126.883	2014	BREA	352
FRK.06	70.084	-126.768	2014	BREA	126
SMO.01	69.860	-126.743	2014	BREA	42
FRK.05	70.082	-126.426	2014	BREA	225
BNK.06	72.929	-126.396	2014	BREA	55
FRK.04	70.087	-126.044	2014	BREA	202
FRK.03	70.084	-125.861	2014	BREA	126
FRK.02	70.085	-125.420	2014	BREA	73
FRK.01	70.081	-125.199	2014	BREA	32
WIS.01	70.102	-125.067	2014	BREA	54
WIS.02	70.175	-124.832	2014	BREA	44
CPY.03	70.444	-124.522	2014	BREA	173
CPY.02	70.259	-124.509	2014	BREA	69.1
CPY.01	70.227	-124.494	2014	BREA	42.7
BPT.01	69.705	-123.821	2014	BREA	41
BPT.02	69.701	-123.785	2014	BREA	71
BPT.04	69.697	-123.239	2014	BREA	68.1
ALX.01	71.617	-120.334	2014	BREA	46.9
AMN.01	70.836	-119.772	2014	BREA	257
PWS.01	72.109	-119.433	2014	BREA	105.3
DOL.01	69.380	-118.764	2014	BREA	184.7
WLK.01	71.480	-118.692	2014	BREA	100
MNT.01	71.228	-118.373	2014	BREA	214.0
WLK.02	71.548	-118.260	2014	BREA	59.4
DOL.03	69.537	-118.220	2014	BREA	437
WLK.03	71.596	-118.008	2014	BREA	45
MNT.04	71.397	-117.191	2014	BREA	75

Table A2. R^2 and p-values from non-transformed and transformed variables in linear regression models. *A transformation for $\delta^{15}N$ was investigated due to the close to significant p=value prior to transformation. Linear regression models were used to investigate the correlation between variables. Both transformed and non-transformed data (Table A2) were used because linear regressions require a normal distribution of the resulting linear model, not necessarily the objects being investigated. Variables that were not transformed were treated as such, either because they were normally distributed (N) or an appropriate transformation wasn't identified NTf (No Transformation) in Table A2.

Environmental data	R^2	p-value	TfR^2	Tf p-value
Depth ~ Salinity*	0.54	2.07e-14	0.85	2.2e-16
Depth ~ Temp	0.16	2.0e-04	0.086	0.0057
Depth ~ Chl-*a*	-0.00086	0.34	-0.15	2.41e-04
Depth ~ Phaeopigment	0.070	0.011	0.021	0.11
Depth ~ Chl-*a* / Phaeo	-0.0084	0.55	-0.011	0.70
Depth ~ δ15N	0.1328	6.6e-04	0.1702	1.1e-04
Depth ~ δ13C*	0.0081	0.21	0.014	0.153
Depth ~ C/N	0.15	2.4e-04	0.2341	4.95e-06
Depth ~ TOC*	-0.0070	0.50	0.010	0.1871
Salinity* ~ Temp	0.18	8.7e-05	0.18	6.2e-05
Salinity* ~ Chl-*a*	0.015	0.15	0.1183	0.0013
Salinity* ~ Phaeopigment	0.035	0.056	0.020	0.11
Salinity* ~ Chl-*a* / Phaeo	0.0068	0.22	0.0064	0.23
Salinity* ~ δ15N	0.1069	0.002	0.096	0.0036
Salinity* ~ δ 13C*	0.038	0.050	NTf	NTf
Salinity* ~ C/N	0.17	1.0e-04	0.20	2.3e-05
Salinity* ~TOC*	0.0055	0.24	NTf	NTf
Temp ~ Chl-*a*	0.0028	0.28	-0.013	0.86
Temp ~ Phaeopigment	0.019	0.12	0.01	0.19
Temp ~ Chl-*a* / Phaeo	9.0e-04	0.34	1.7e-04	0.32
Temp ~ δ15N	0.0092	0.20	0.0080	0.20
Temp ~ δ13C*	0.067	0.013	0.067	0.013
Temp ~ C/N	0.11	0.0017	0.12	0.0011
Temp ~TOC*	0.010	0.19	0.0055	0.24
Chl-*a* ~ Phaeopigment	0.26	1.4e-06	0.50	4.25e-13
Chl-*a* ~ Chl-*a* / Phaeo	-0.010	0.65	-0.013	0.96
Chl-*a* ~ δ15N	-0.008	0.56	0.089	0.005
Chl-*a* ~ δ 3C*	0.036	0.055	0.11	0.0021
Chl-*a* ~ C/N	-0.012	0.80	0.0082	0.21
Chl-*a* ~TOC*	0.032	0.065	0.091	0.005
Phaeo ~ Chl-*a* / Phaeo	0.015	0.14	0.079	0.0077
Phaeopigment ~ δ15N	-0.0036	0.40	-0.0022	0.37
Phaeopigment ~ δ13C*	0.15	3.4e-04	0.18	8.1e-05
Phaeopigment ~ C/N	0.032	0.064	0.015	0.15
Phaeopigment ~TOC*	0.0086	0.20	0.0056	0.24
Chl-*a* / Phaeo ~ δ15N	-0.0060	0.46	0.017	0.13
Chl-*a* / Phaeo ~ δ13C*	-0.013	0.94	-0.0082	0.54
Chl-*a* / Phaeo ~ C/N	-0.012	0.79	-0.079	0.0078
Chl-*a* / Phaeo ~TOC*	-0.012	0.79	0.038	0.050
δ15N ~ δ13C*	0.10	0.0029	0.10	0.0020
δ15N ~ C/N	0.070	0.011	0.11	0.0019
δ15N ~TOC	-0.013	1.0	-0.013	0.89

Table A3. R_s and p-values from Spearman's Rho investigation of correlations between environmental variables.

Note that "abs"= absolute value.

R_s	**Dep(m)**	**Chl-*a***	**Phaeo**	**Ch/Ph**	**δ 15N**	**absδ^{13}C**	**C/N**	**TOC**	**Temp**	**Sal**
Depth	1	-0.39	0.17	-0.76	0.42	-0.05	-0.52	-0.19	0.37	0.94
Chl-*a*	-0.39	1	0.69	0.43	-0.36	0.49	0.18	0.37	0.03	-0.33
Phaeo	0.17	0.69	1	-0.3	-0.12	0.47	-0.13	0.15	0.13	0.2
Ch/Ph	-0.76	0.43	-0.3	1	-0.25	0.02	0.48	0.34	-0.2	-0.7
δ^{15}N	0.42	-0.36	-0.12	-0.25	1	-0.55	-0.4	-0.02	0.14	0.39
abs(δ^{13}C)	-0.05	0.49	0.47	0.02	-0.55	1	-0.2	0.36	0.15	0.02
C/N	-0.52	0.18	-0.13	0.48	-0.4	-0.2	1	0.09	-0.31	-0.47
TOC	-0.19	0.37	0.15	0.34	-0.02	0.36	0.09	1	0.01	-0.1
Temp	0.37	0.03	0.13	-0.2	0.14	0.15	-0.31	0.01	1	0.41
Salinity	0.94	-0.33	0.2	-0.7	0.39	0.02	-0.47	-0.1	0.41	1
p-values	**Dep(m)**	**Chl-*a***	**Phaeo**	**Ch/Ph**	**δ 15N**	**absδ^{13}C**	**C/N**	**TOC**	**Temp**	**Sal**
Depth		0.00	0.14	0.00	0.00	0.68	0.00	0.09	0.00	0.00
Chl-*a*	0.00		0.00	0.00	0.00	0.00	0.11	0.00	0.80	0.00
Phaeo	0.14	0.00		0.01	0.28	0.00	0.26	0.19	0.28	0.09
Ch/Ph	0.00	0.00	0.01		0.03	0.85	0.00	0.00	0.08	0.00
δ^{15}N	0.00	0.00	0.28	0.03		0.00	0.00	0.85	0.22	0.00
abs(δ^{13}C)	0.68	0.00	0.00	0.85	0.00		0.08	0.00	0.21	0.85
C/N	0.00	0.11	0.26	0.00	0.00	0.08		0.43	0.01	0.00
TOC	0.09	0.00	0.19	0.00	0.85	0.00	0.43		0.91	0.37
Temp	0.00	0.80	0.28	0.08	0.22	0.21	0.01	0.91		0.00
Salinity	0.00	0.00	0.09	0.00	0.00	0.85	0.00	0.37	0.00	

Chukchi-Beaufort Seas Storms and Their Influence on Surface Climate

Principal Investigator: Yang Yang

International Arctic Research Center
University of Alaska Fairbanks

Cooperative Agreement Number: M16AC00007
Period of Performance: 6/16-1/18

Contents

List of Figures

Abstract

The storms that enter the Chukchi Sea and western Beaufort Sea region originate predominantly from the Pacific Ocean, possibly as far south as the sub-tropical Pacific region, or from the East Siberian Sea region. These storms take two primary pathways into the Chukchi and western Beaufort Seas: south to north from the Pacific Ocean (S2NP storms) and west to east from the East Siberian Sea (W2E storms). These storm types have distinct characteristics and can produce substantial local and regional changes in surface atmospheric and oceanic properties. In this study, the climatology of these two types of storms was analyzed using the Chukchi-Beaufort High-Resolution Atmospheric Reanalysis (CBHAR) dataset. The results show that the W2E and S2NP storms have the most prominent influences on surface climate and ocean properties in August and October, respectively, and that the S2NP storms are generally stronger than the W2E storms. The composite analysis of 2 m temperature fields, based on the number of S2NP storms, indicates a strong thermal contrast along the coast and suggests the occurrence of a baroclinic zone that supports storm development. The composite analysis of surface winds demonstrates that W2E storms change prevailing weak northeasterly winds to strong southerly winds over the Bering and Chukchi Seas and southerly surface winds occur on the northern coast of Alaska when the S2NP storms enter the study domain. The S2NP storms bring warm and moist air from the Pacific Ocean into the Arctic. In climatology, downward longwave and shortwave radiation at the surface are larger than surface turbulent heat fluxes. There are large differences in surface climate variables between the climatological mean and the composite analysis based on the number of storms. The composite analysis also indicates that both surface latent and sensible heat fluxes decrease when storms occur in the study area. It is suggested that storms can reduce sea ice concentration substantially in the ice areas through a combination of thermodynamic and dynamic factors. Sea ice retreat (northward) and sea ice advancement (southward) occur with southerly and northerly winds induced by the storms entering the study domain. Possible linkages were suggested between sea ice anomalies and frequency of the S2NP storms over the region.

Introduction

The Arctic has experienced significant environmental changes including rapidly decreased sea ice cover and considerably increased ocean and air temperatures (Comiso et al., 2008; Steele et al., 2008; Screen and Simmonds, 2010). Recent research has found an intensification of synoptic storm activity over the Arctic Ocean (e.g., Zhang et al., 2004; Serreze et al., 2008; Simmond et al., 2008; Woods and Caballero, 2016; Graham et al., 2017). As one outstanding example, a superstorm invaded the Beaufort-Chukchi Seas from eastern Siberia in August 2012, contributing to record low summer sea ice coverage (Simmonds and Rudeva, 2012). In 2016, the Korean icebreaker *Araon* observed an extreme storm moving from the East Siberian Sea into the Chukchi Sea, rapidly reducing the sea ice extent in that area. With diminishing sea ice cover and more open water, we will likely observe increased frequency and intensity of storms, changes in surface wind patterns, and increased surface wind speeds and precipitation. The communities along the coast of Alaska would be subject to the threat of extreme weather events caused by intense storms, which increase the potential for coastal erosion and flooding.

The spatial resolution in previous Arctic storm studies ranged from 50 km to 200 km, which may not resolve high-resolution geometrical features of storms. Little research has been undertaken using fine-resolution data to document the climatological characteristics of storms in the Chukchi and Beaufort Seas or to investigate how the storms influence surface climate. The Chukchi-Beaufort High-Resolution Atmospheric Reanalysis (CBHAR) has horizontal resolutions of 10 km for each hour from 1979 to 2009, which makes it possible to analyze high-resolution climatology features of synoptic storms and their influences on surface climate and ocean properties.

Though the climatological wind direction in the Chukchi and Beaufort Seas region is easterly, storms propagate into the study domain moving south to north from the Pacific Ocean (S2NP) and west to east (W2E) from eastern Siberia. The S2NP storms are most likely to migrate up through the Bering Sea. In this study, we assessed how these two storm groups influenced the surface climate. This study aimed to document climatological features of the storms that travel along different pathways.

Methods

This study was based on the 31-year, 10-km horizontal, hourly Chukchi-Beaufort High-Resolution Atmospheric Reanalysis (CBHAR) (Liu et al., 2014; Zhang et al., 2013). The Advanced Research Weather Research and Forecasting model (WRF-ARW; Skamarock et al. 2008) was the main tool for generating this reanalysis dataset. CBHAR is a three-dimensional observationally constrained and thermodynamically and dynamically consistent gridded hindcast reanalysis. It covers the Chukchi and Beaufort Seas, the Arctic Slope of Alaska and the Brooks Range, the western part of the Canadian Yukon Territory, and the East Siberian Sea coastal area (Figure 1). The initial and lateral boundary conditions are from The European Centre for Medium-Range Weather Forecasts Interim Re-Analysis (ERA-Interim; Dee et al. 2011). The high spatial resolution allows CBHAR to resolve fine scale synoptic storm processes and their impact on the surface variables and ocean properties.

HIRHAM-NAOSIM is a regional coupled atmospheric-ocean-ice model that covers the Arctic region north of approximately 60°N (Rink et al., 2003, 2013) (Figure 1). HIRHAM is a regional atmospheric climate model based on a subset of the High-Resolution Limited Area Model (HIRLAM; Unden et al. 2002) and the ECHAM climate model (Roeckner at al. 2003). HIRHAM is the atmospheric component of the coupled model and has a horizontal resolution of 50 km. The North Atlantic-Arctic Ocean Sea Ice Model (NAOSIM) is the ocean-ice component of the coupled model and has a horizontal resolution of approximately 25 km. We compared the CBHAR results with output from the HIRHAM-NAOSIM to show that characteristics of Chukchi Sea and Beaufort Sea storm climatology are rather different from the HIRHAM-NAOSIM results.

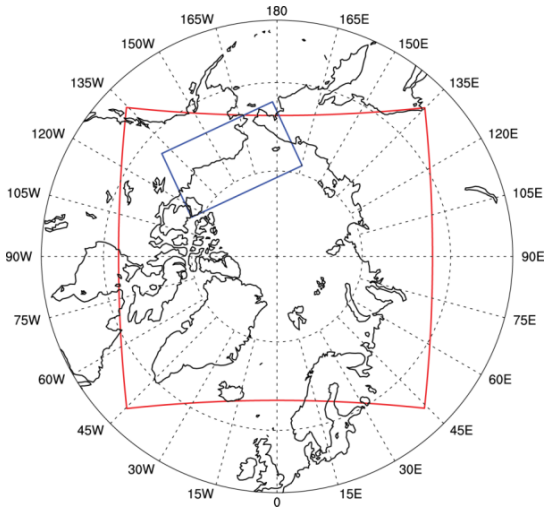

Figure 1. Extent of CBHAR (blue) and HIRHAM (red) domains.

We applied and refined the automatic storm identification and tracking algorithm developed by Zhang et al. (2004) using 6-hourly sea-level pressure (SLP) fields to track the storms. The criteria for identifying and tracking storms included the following:

(1) A storm center was identified if the SLP at the grid point was lower than all surrounding grid points within a 50 km radius using the CBHAR data.

(2) The minimum SLP between the center of the storm and every surrounding grid point was at least 0.01 hPa.

(3) Two adjacent storm centers appearing concurrently within 500 km of each other were identified as the same storm system with the lowest storm center as the center of the combined storm system.

(4) The lifetime of the storm was at least 12 hours, and each storm track was at least 100 km long. The latter criteria eliminated minor disturbances generated by orographic effects.

Using the criteria above, we identified 451 storms traveling into the Chukchi and Beaufort Seas from 1979 to 2009: 290 individual storms as S2NP and 161 as W2E. Figure 2 depicts the composite tracks associated with the S2NP storms and the W2E storms.

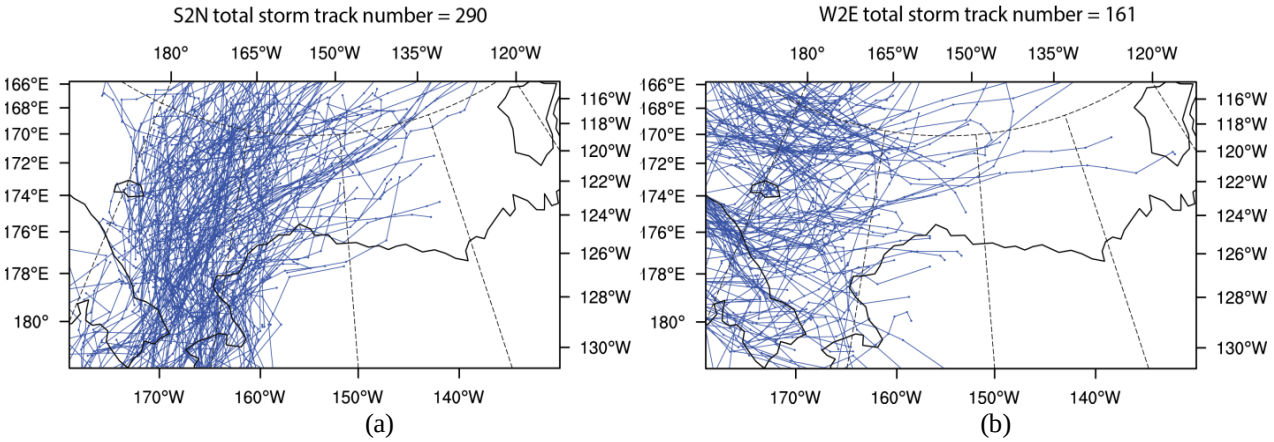

Figure 2. Storm track clusters of (a) the S2NP and (b) the W2E storms from 1979 to 2009. The blue lines are individual storm paths.

To investigate the characteristics of storms moving into the Chukchi and Beaufort Seas from these two pathways, we performed a composite analysis for each set of the S2NP and W2E storms. Using CBHAR data, we calculated the average SLP fields for each storm and used that data to calculate the average for the S2NP and W2E storms, respectively, for the period 1979–2009.

Storm intensity, duration, and track number were calculated. The storm intensity was obtained by calculating the mean absolute values of the difference between the central SLP of the storm and the climatological monthly mean SLP at the corresponding grid points over the cyclone duration. Intensities of storms in the month were averaged to get monthly mean absolute values. The storm

track count was the number of storms moving in a particular geographical region in a month. The storm duration was the length of time between the first appearance of the storm and its subsequent disappearance. The average storm duration was obtained by averaging the storm durations within each region.

Climatologically, Arctic storms are not active in summer, and it is widely acknowledged that Arctic storms are typically more intense in winter. However, we found the S2NP and W2E storms were most dominant in October and August, respectively, so these months are the focus of this composite analyses performed for 2 m surface air temperatures, 10 m winds, sea surface temperature (SST), sea ice concentrations, and the following energy budget terms: downward longwave radiation, downward shortwave radiation, surface sensible heat flux, and surface latent heat flux. Composite analysis eliminates the details of individual storms from the dataset, leaving only the general features for storms along a specific path.

Results

Storm Seasonality

Significant differences exist in the seasonal cycle of the S2NP and W2E storms (Figure 3). W2E storms have a pronounced seasonal cycle. Over the 31-year period, the number of W2E storms averaged 34 and 2 for August and January, respectively, and storm intensity, duration, and track number all peaked in August. The lifetime of the W2E storms is longer in summer months and shorter in the other seasons when compared to the S2NP storms. A seasonal cycle of storm duration and track numbers is not as evident for the S2NP storms. The number of the S2NP storms ranged between 20–30 per month and was relatively consistent throughout the year. Storm intensity was greater for the S2NP compared with the W2E storms throughout the year; however, S2NP storm intensities reflected only a moderate seasonal cycle, higher in winter and lower in summer, which is consistent with the Pan-Arctic storm intensity seasonal cycle from the HIRIHAM-NAOSIM output (Figure 4). The highest values in the S2NP storm intensity, duration, and track number all occurred in October.

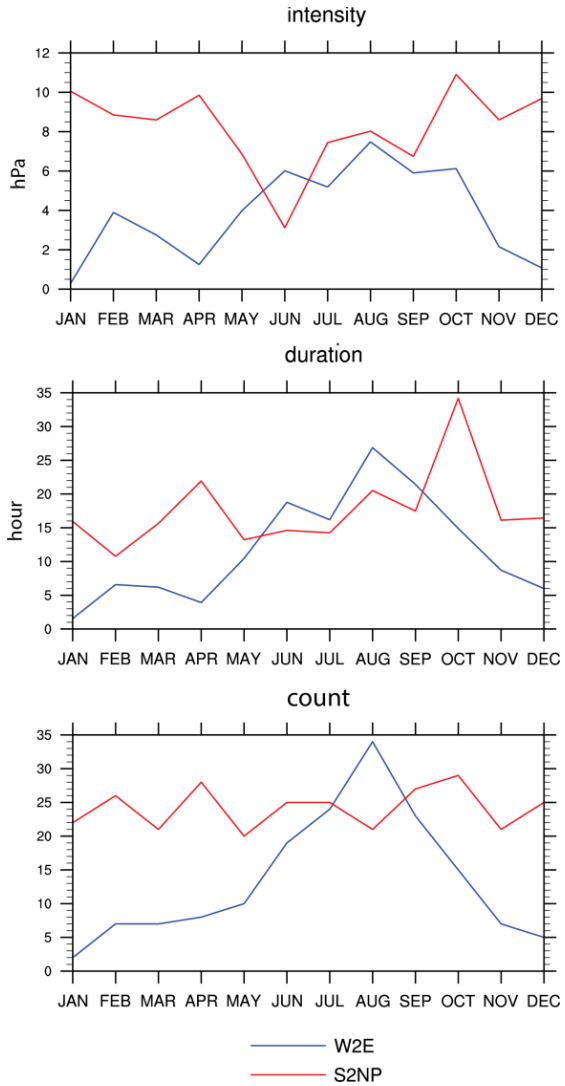

Figure 3. Seasonal cycle of intensity, duration, and count for the W2E (blue line) and the S2NP (red line) storms from 1979 to 2009

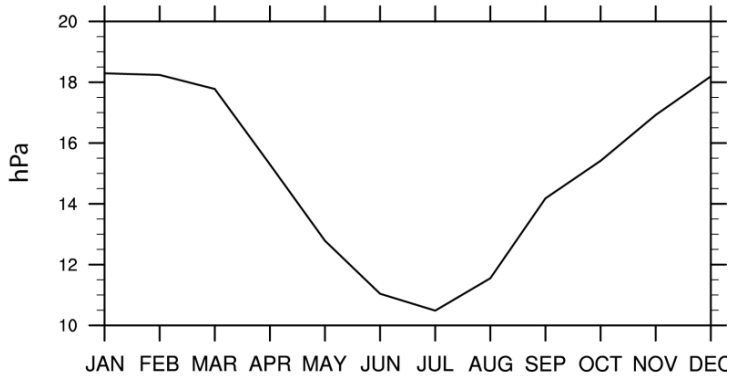

Figure 4. Seasonal cycle of intensity for the Pan-Arctic storms in the HIRHAM domain from 1979 to 2014.

Composite Analysis of Surface Climate

Sea-level pressure

The sea-level pressure (SLP) difference is notably large between the climatology and both storm composites. Climatologically, the SLP field is characterized by a weak high-pressure system over the Beaufort Sea near the Alaskan coast in August (Figure 5a). In contrast, the W2E storm composite SLP field is characterized by a low-pressure system near 73°/180°E in the East Siberian Sea, which produces a strong pressure gradient parallel to the coast favorable for northwesterly flows. Lower than normal pressure covers the western Beaufort Sea and the East Siberian Sea. Figure 5b reveals clear distinctions between the climatology and the S2NP storm composite SLP field in October. The main passage of the S2NP storms approaching the Chukchi and Beaufort Seas is through Bering Strait, where storm occurrences are persistent throughout the year (Figure 3). A closed contour of low pressure is evident in the Bering Strait in the S2NP storm composite SLP field, and the wind changes direction when storms occur. As shown in Figure 6, the easterly wind parallel to the Alaska coast changed to southerly offshore wind. This indicates that offshore flow is more frequent with S2NP storms passing through Bering Strait in October. Cyclonic flow over the East Siberian Sea is conducive for warm and moist air advection in the Bering Strait and possibly onshore over the Brooks Range. The wind resulting from the intense S2NP storms would be southwesterly through the Bering Strait and southerly along the Beaufort Sea coast, increasing open water near shore.

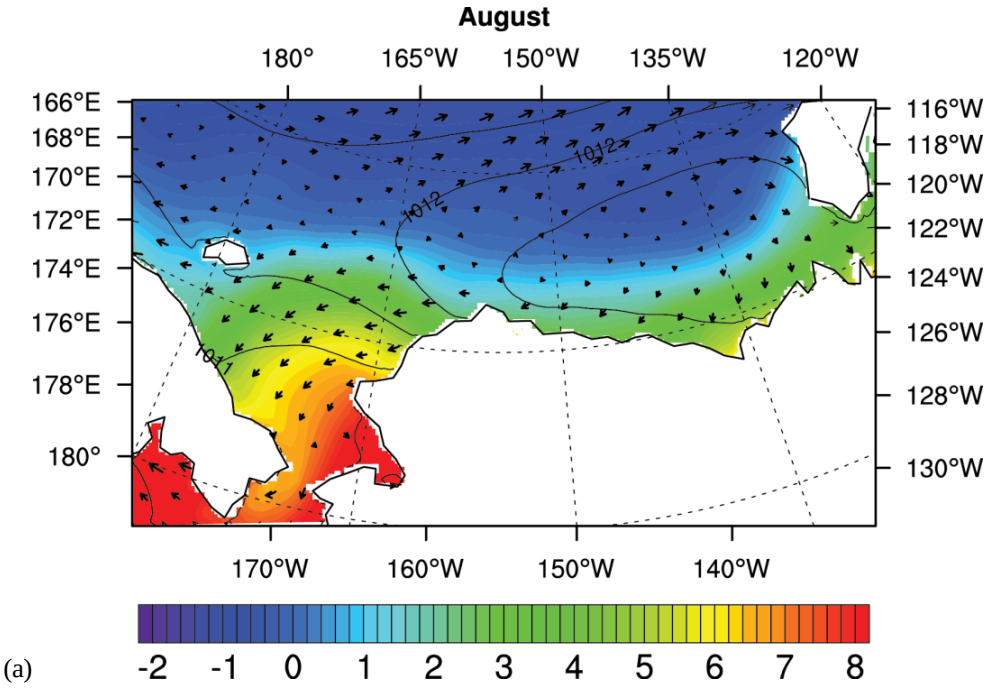

(a)

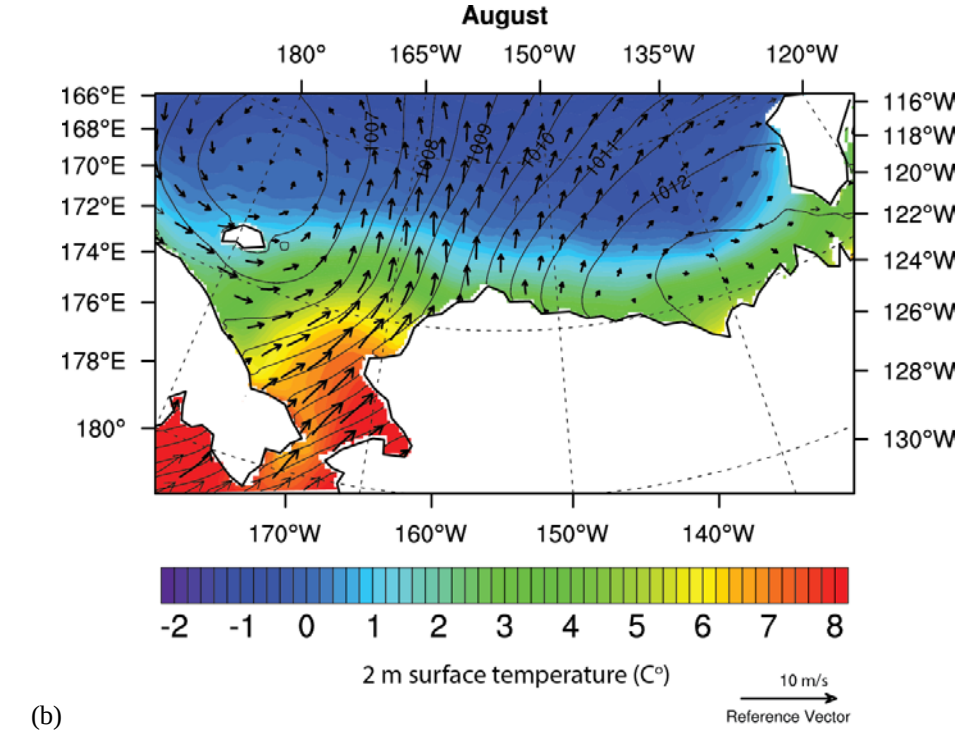

(b)

Figure 5. (a) Climatological and (b) W2E storm composite SLP (black contour), 2 m surface air temperature (color fill), and 10 m wind vector for August.

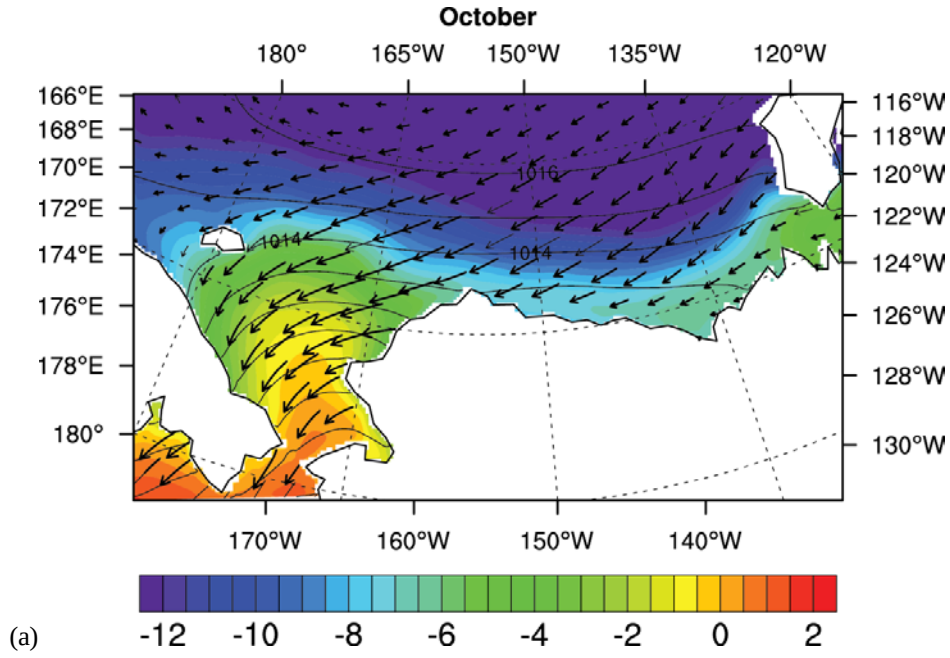

(a)

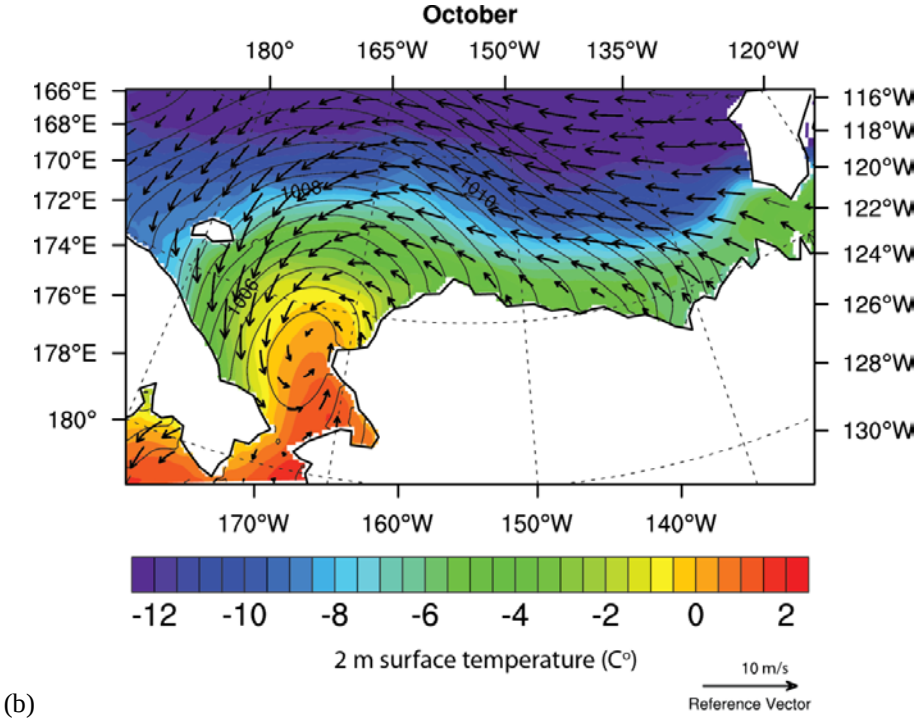

(b)

Figure 6. (a) Climatological and (b) S2NP storm composite SLP (black contour), 2 m surface air temperature (color fill) and 10 m wind vector for August.

10 m wind

Climatological and storm composites of the 10 m wind speed fields for the W2E storms are shown in Figure 7. Climatologically, the August wind is rather calm in the Chukchi and Beaufort Seas area (Figure 5a). W2E storms can bring strong southwesterly winds into the Chukchi and Bering Seas. This strong offshore flow blowing from the east Eurasian landmass can advect positive temperature anomalies, contributing to warming over the coastal area of the East Siberian and Bering Seas. The W2E storms can cause intense wind events in Bering Strait and the adjacent Chukchi Sea. Instead of a climatological weak northeasterly wind along the coast of the East Siberian Sea, Figure 7b shows a region of increased westerly flows along the coast and enhanced wind speeds. The difference between the climatological mean wind speed field and that of the storm composite field is shown in Figure 7c. For both storm types, the maximum 10 m surface wind speed increase is found along the coast of the East Siberian Sea and in the Bering Strait.

Climatological and storm composites of the 10 m wind speed fields for the S2NP storms and their difference are shown in Figure 8. The S2NP composite 10 m wind field is also quite different from the climatological wind field (Figure 6). The prevailing wind in October is easterly in Chukchi and Beaufort region. Strong easterly flows dominating the October Chukchi and Beaufort wind fields are no longer present in the S2NP storm composite wind field (Figure 8b). Instead, there are strong southerlies and south-westerlies in the regions blowing in the offshore direction. There is a moderate increase in wind speed in the East Siberian Sea and the Chukchi Sea and a decrease in wind speed in the Bering Strait.

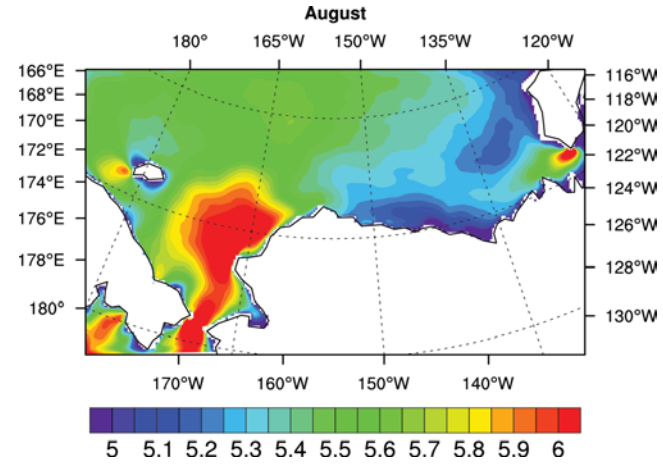

(a)

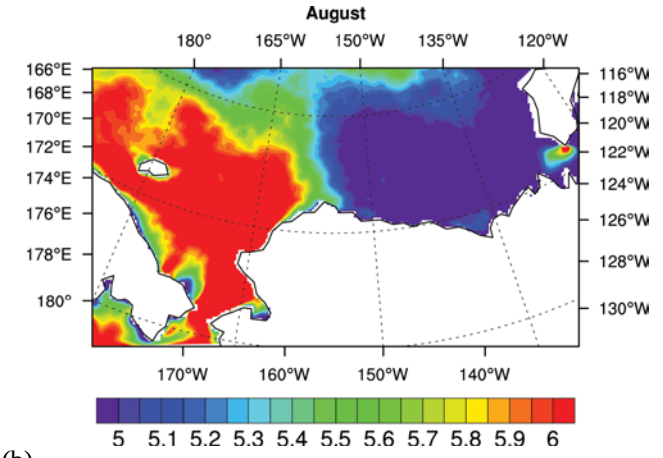

(b)

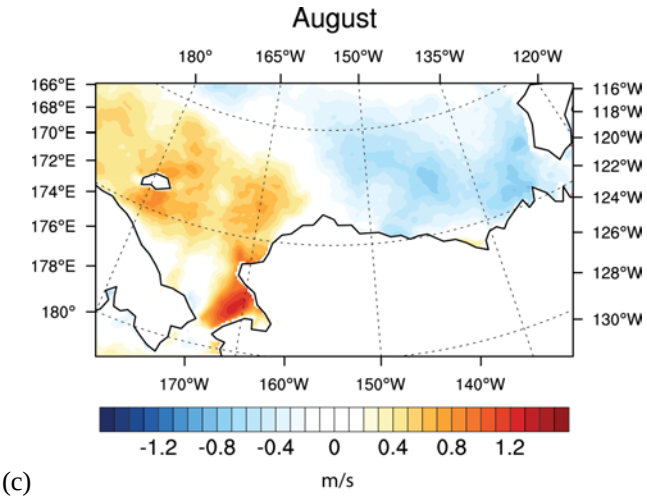

(c)

Figure 7. (a) Climatological and (b) W2E storm composite wind speed. (c) Difference between the W2E storm composite and climatological wind speed field.

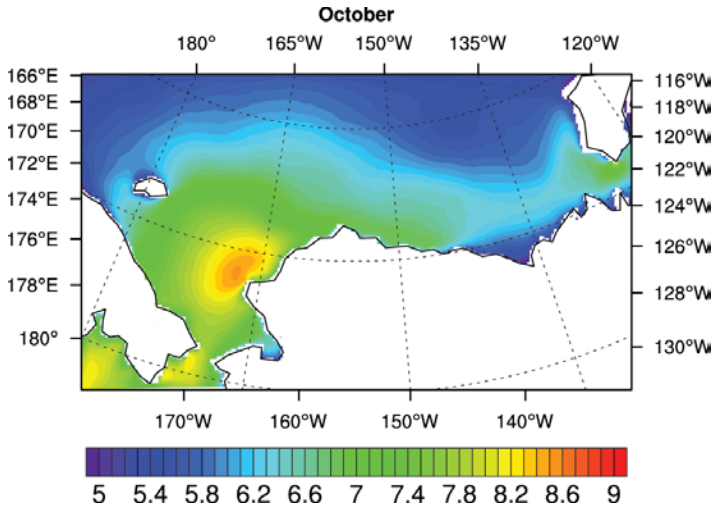

(a)

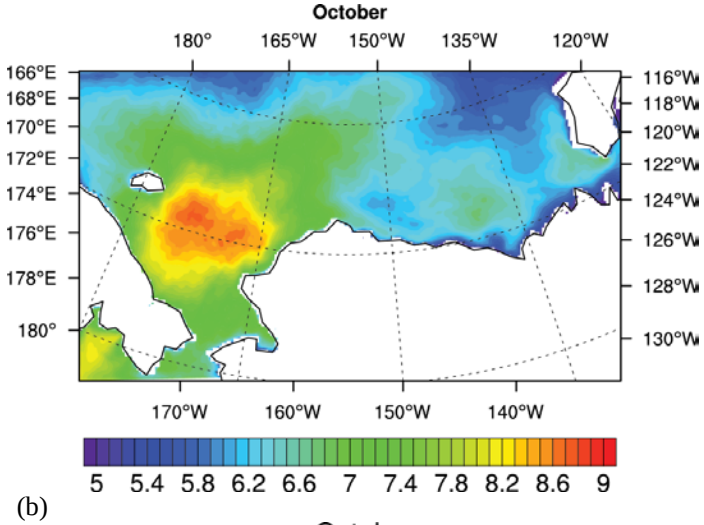

(b)

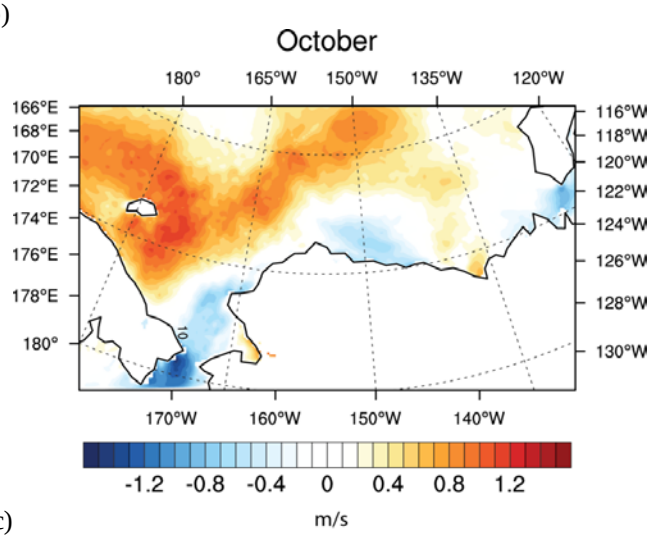

(c)

Figure 8. (a) Climatological and (b) S2NP storm composite wind speed. (c) Difference between the S2NP storm composite and climatological wind speed field.

2 m surface air temperature

The climatological 2 m surface air temperature and 10 m surface winds in August are shown in Figure 9a. The August 2 m surface air temperatures over the north part of Chukchi and Beaufort Seas are around the freezing point due to the melting of sea ice. There is sharp discontinuity of 2 m temperature stretching from the Siberian coast across the Chukchi and Beaufort Seas due to differential heating of the atmosphere between the land and the ice-free ocean (Figure 9a). The large temperature gradient in August suggests the presence of a baroclinic zone along the coast. Migrating storms can bring temperature changes through horizontal temperature advection (Figure 9b). The dominant features for the storm composite 2 m surface temperature are warming along the coastal areas of the East Siberian Sea and the Alaskan sector southern boundary of the Beaufort Sea and cooling over the Canadian sector southern Beaufort Sea. The August offshore southerlies yield warmer than climatological temperatures over the northeastern East Siberian Sea, southern Chukchi Sea, and the Bering Sea. The difference between the climatological and storm composite 2 m surface temperature field is relatively small (Figure 9c).

Climatologically, easterly winds in October are associated with cold air advection over the coastal area of northern Alaska. Onshore flow tends to advect cool air to land, and cold air advection is dominant along the Alaskan Beaufort Sea coastal area. The land is colder than the open water area along the Beaufort coast, and the North Slope area is dominated by temperatures below -10°C (Figure 10a). Northeasterly winds advect cold air over the Beaufort Sea toward the Alaskan coastal region, yielding strong negative temperature anomalies along the coast. Figure 10b provides the S2NP storm October composite of the 2 m surface air temperature field with 10 m wind vectors. There is a substantial increase of surface temperature in the North Slope region in comparison to climatological values. This indicates that the S2NP storms can advect warm air from the south into the North Slope regions. Prominent warm temperature anomalies are also present in Bering Strait. Most of the Beaufort Sea is characterized by warming of 2 m surface temperatures when S2NP storms occur (Figure 10b). There are smaller temperature contrasts between the land and ocean when the S2NP storms bring southerly flow over the Brooks Range. There is a clear correspondence between the area of negative temperature anomalies associated with northerly winds in the East Siberian Sea. Temperature increases caused by the October S2NP storms along the Beaufort coast are over 2.5°C higher than the increases brought by the W2E storms in August (Figure 10c).

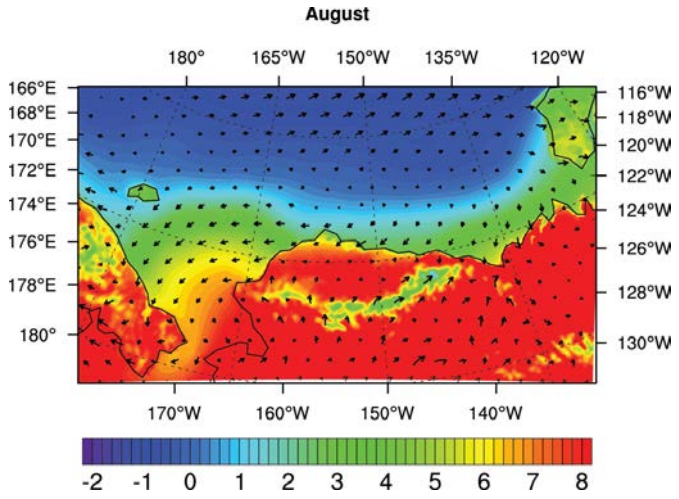

(a)

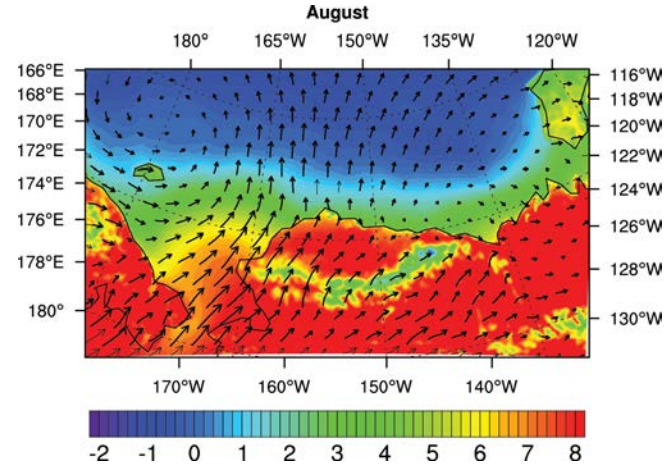

(b)

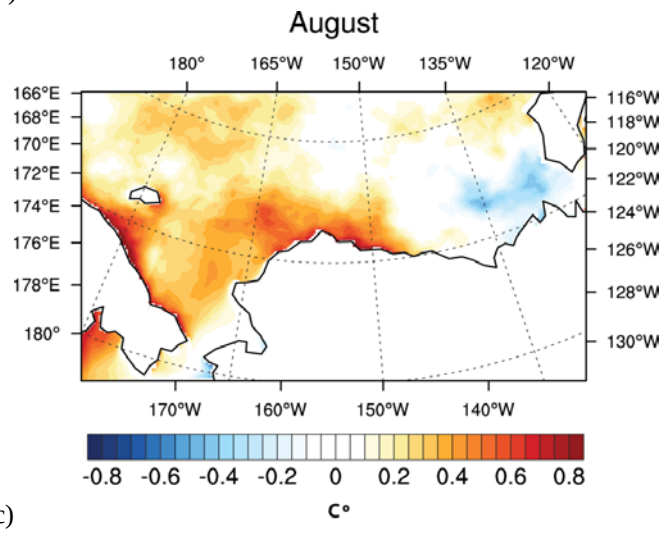

(c)

Figure 9. (a) Climatological and (b) W2E storm composite 2 m surface temperature. Black arrows indicate wind vectors. (c) Difference between the W2E storm composite and climatological 2 m surface temperature.

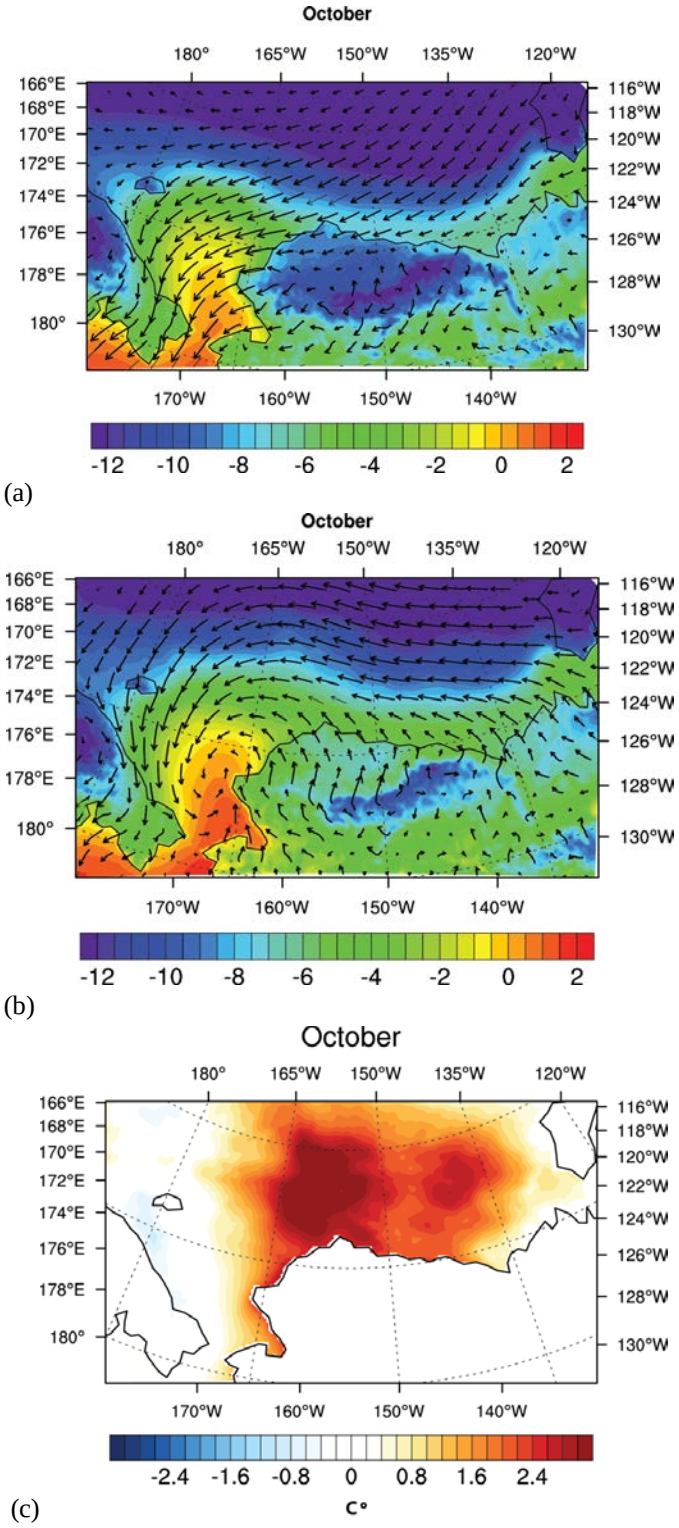

Figure 10. (a) Climatological and (b) S2NP storm composite 2 m surface temperature. Black arrows indicate wind vectors. (c) Difference between the S2NP storm composite and climatological 2 m surface temperature.

Sea surface temperature

In general, the pattern for the climatological sea surface temperature (SST) field is similar to that for the storm composite SST field (Figures 11a and 11b, respectively). A common feature of the climatological and storm composite SST fields is the warm water in Bering Strait and the sharp SST gradient in the Bering Sea in August. During the W2E storm events, slight increases of SST are observed along the Beaufort coast of Alaska and eastern Siberia coast (Figure 11c). The SST change in the Bering Sea is very small, even though this region corresponds to wind speed increases and wind direction changes when the W2E storms occur. Similar to the W2E storms, the S2NP storm composite SST fields resemble that of the October climatological pattern (Figure 12b and 12a, respectively) in that the highest SST is centered in the Bering Strait with a large SST gradient present. In contrast to the W2E, the SST decreases along the coast of the East Siberian Sea in the S2NP storm scenario (Figure 12c).

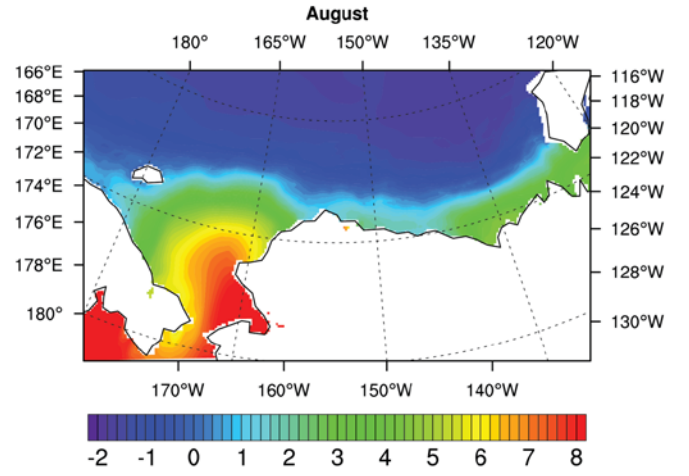

(a)

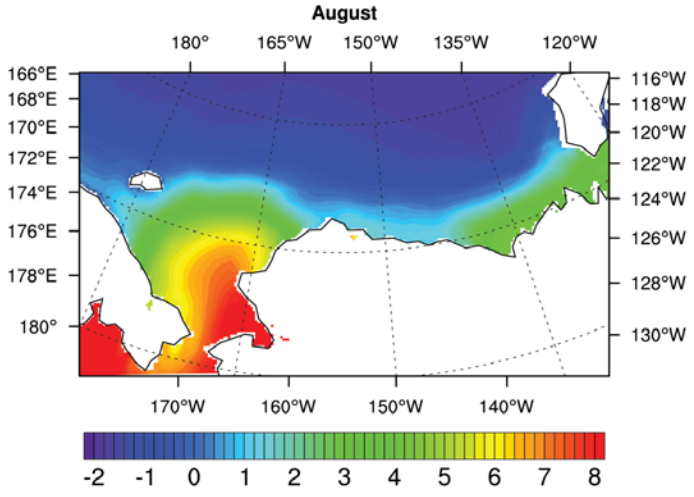

(b)

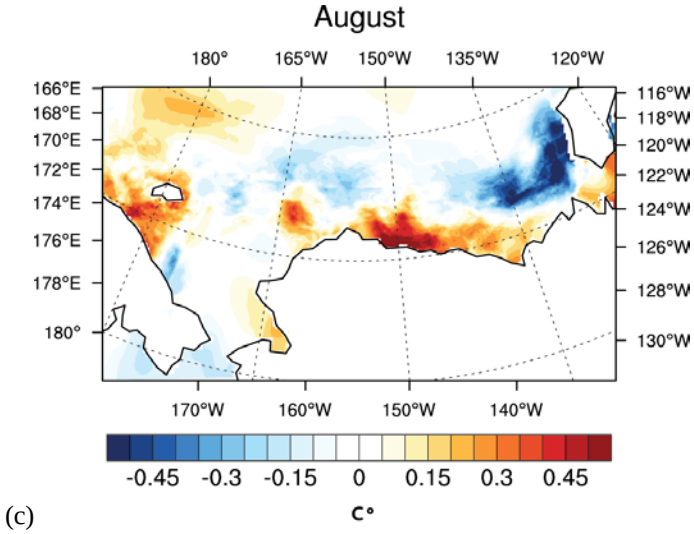

(c)

Figure 11. (a) Climatological and (b) W2E storm composite SST. (c) Difference between the W2E storm composite and climatological SST.

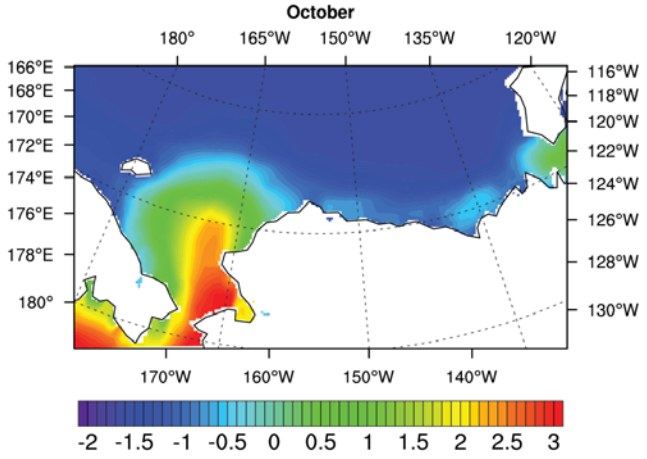

(a)

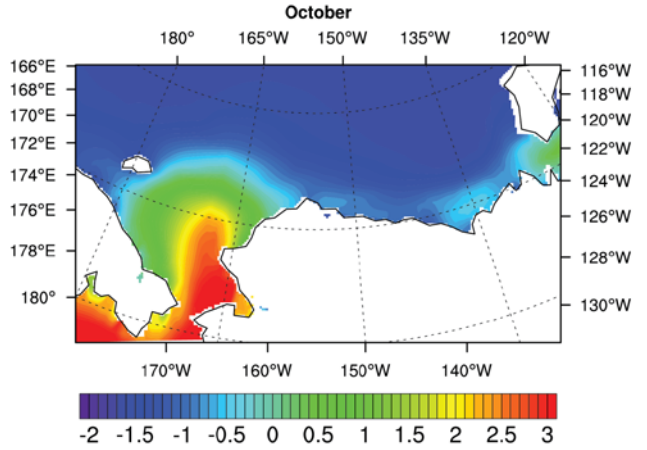

(b)

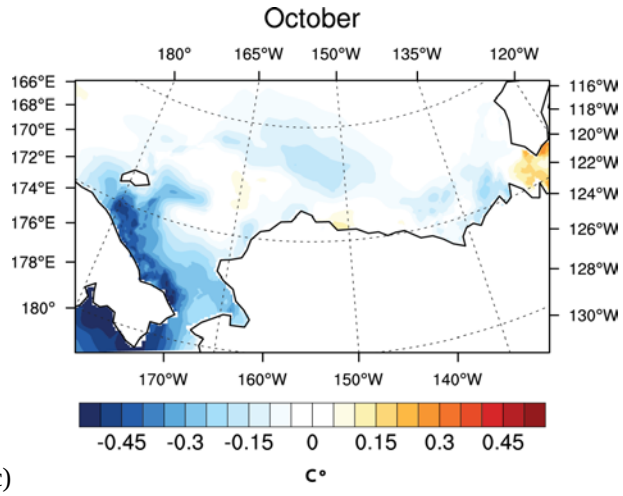

(c)

Figure 12. (a) Climatological and (b) S2NP storm composite SST. (c) Difference between the S2NP storm composite and climatological SST.

Sea ice concentration

Changes in temperature, wind speed, and wind direction caused by storms can have direct impacts on the changes of sea ice. Serreze et al. (1995) proposed linkages between large anomalies in summer sea ice extent and a high frequency of cyclone activity. In this section, we will examine the change of sea ice concentration when different storms occur.

The southern Beaufort Sea coastal areas are normally ice-free in August, but northern areas in deeper water and off the shelf are consistently covered by sea ice. This has obviously changed over the last ten years. When the W2E storms dominate the Chukchi Sea in August, the 10% sea ice concentration contour slightly advances southward near the coast of the East Siberian Sea and retreats northward in the eastern Chukchi Sea (Figure 13a), which corresponds to the northerly and southerly wind vectors of the W2E storms (Figure 9b). Wendler (1973) showed that sea ice conditions depend on the surface wind direction. Strong southwesterly wind can bring the warm continental air to the East Siberian Sea and the Chukchi Sea and melt the sea ice. In early October, the sea ice begins to freeze up. There is a sharp decrease of sea ice when the S2NP storms progress into the Chukchi and Beaufort Seas area. These decreases are greatest along the Chukchi Sea coast of Alaska and in the eastern Bering Sea (Figure 13b). The pronounced October sea ice concentration reduction is located within 100 km offshore of the Alaska Coast in the eastern Chukchi Sea. This area favors polynyas and thin ice, which can be pushed away from the coast by the southerly to southeasterly offshore winds of the S2NP storms even though the prevailing climatological wind direction in this area is from the northeast (Figure 10a). There is no significant 2 m surface air temperature difference between the continent and the adjacent ice-covered ocean (Figure 10b), which suggests wind, not temperature, is influencing sea ice concentration. The S2NP storms over the eastern Chukchi Sea promote warm and moist southerly flows that can enhance melting of sea ice and reduction of surface albedo. This may explain the retreat of the 10% sea ice concentration contour when the S2NP storms are present (Figure 13b).

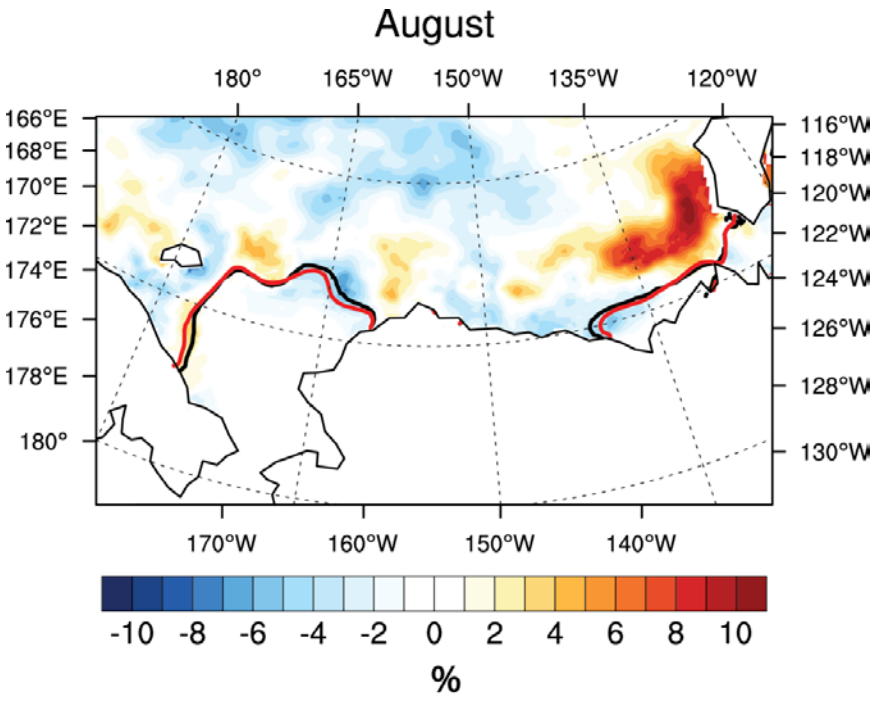

(a)

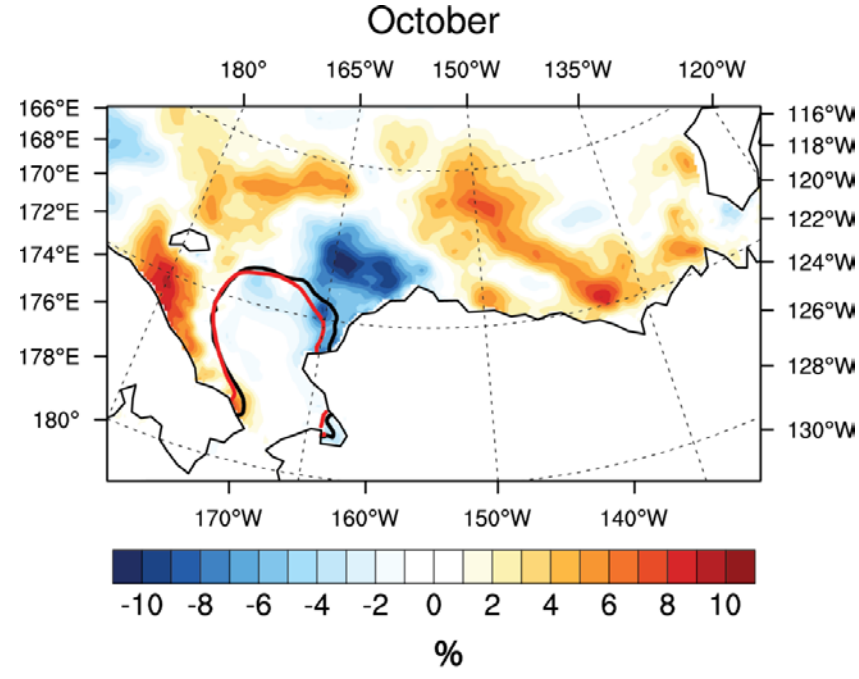

(b)

Figure 13. Difference between the storm composite and climatological sea ice concentration for (a)W2E and (b) S2NP storms. The black and red lines are the storm composite and climatological 10% sea ice concentration contour respectively.

Downward longwave radiation

We examined the atmospheric energy budget of the of the Chukchi and Beaufort Seas for changes in downward longwave radiation linked to W2E and S2NP storm activity (Figures 14 and 15, respectively). Downward longwave radiation is emitted by the atmosphere and is influenced by clouds and water vapor. All positive values are in the upward direction, from ocean to the atmosphere. The increase of downward longwave radiation at the surface is in response to the increase in cloud cover. Increased longwave radiation favors more radiative warming and, therefore, ice melt and heat uptake in the ocean. October is the transition time from summer to winter conditions. Large upward fluxes occur over open water and the coastal Chukchi and Beaufort Seas where thin ice is growing, with smaller upward fluxes occurring over the northern Beaufort Seas where thick sea ice is present. The increase of downward longwave radiation with the S2NP storms in October (Figure 15c) is twice that due to the W2E storms in August (Figure 14c).

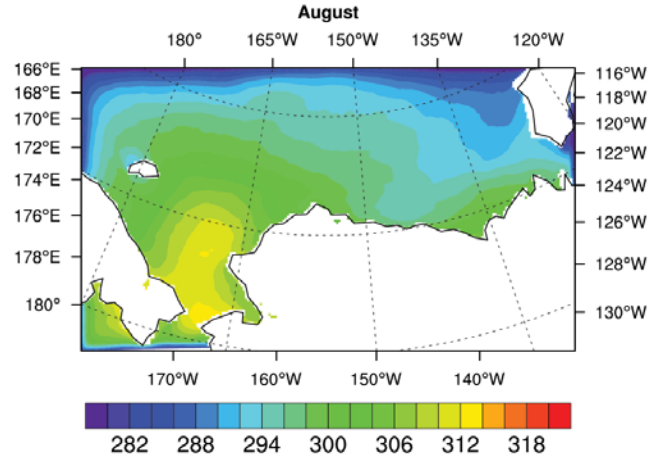

(a)

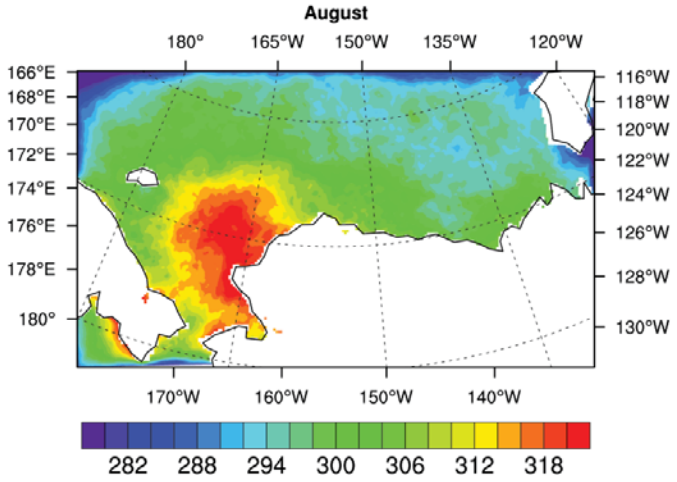

(b)

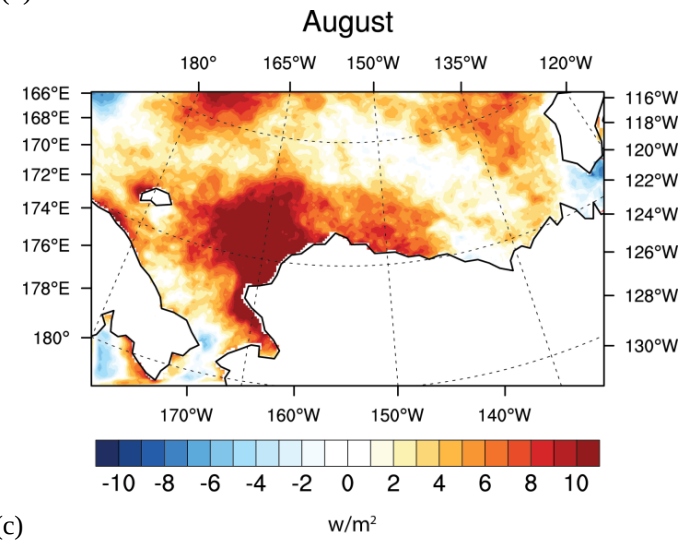

(c)

Figure 14. (a) Climatological and (b) W2E storm composite downward longwave radiation. (c) Difference between the W2E storm composite and climatological downward longwave radiation.

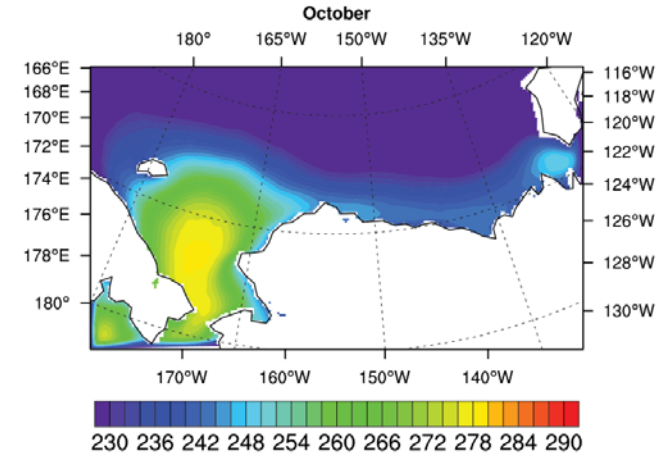

(a)

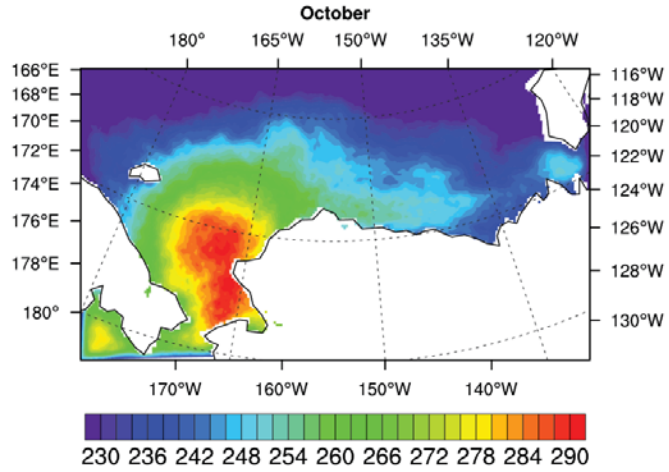

(b)

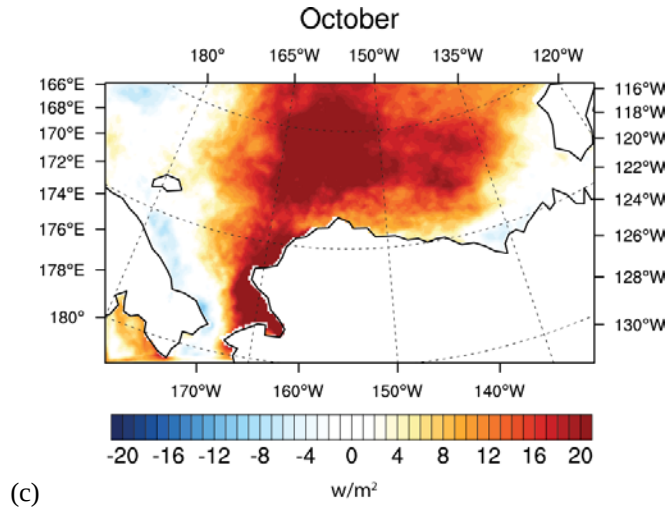

(c)

Figure 15. (a) Climatological and (b) S2NP storm composite downward longwave radiation. (c) Difference between the S2NP storm composite and climatological downward longwave radiation.

Downward shortwave radiation

We examined the atmospheric energy budget of the of the Chukchi and Beaufort Seas for changes in downward shortwave radiation linked to W2E and S2NP storm activity (Figures 16 and 17, respectively). Downward shortwave radiation decreases due to cloud cover associated with storms, reflecting more solar energy back to space (Figure 16a). The greatest reduction of downward shortwave radiation, caused by the W2E storms in August, covers most of the Chukchi Sea region (Figure 16c). Figure 17c illustrates a widespread decrease of downward shortwave radiation due to October S2NP storms, especially in the eastern Beaufort Sea. This area corresponds to the regions with peak values of downward longwave radiation (Figure 15c). There is also a substantial increase of downward shortwave radiation along the coast of the East Siberian Sea, possibly due to the cold air advection from the north clearing the sky over the region.

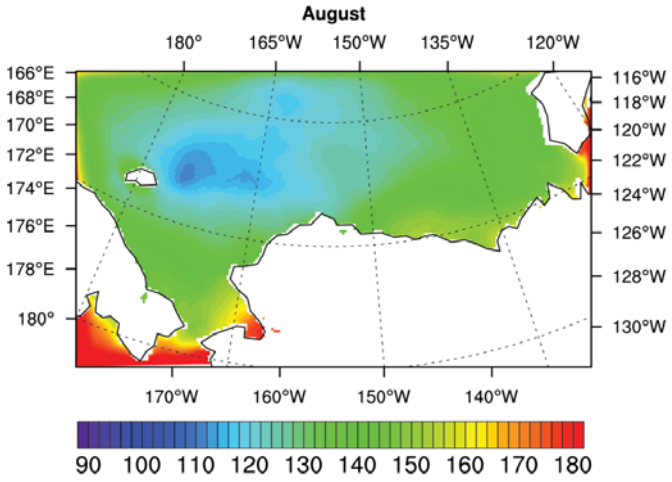

(a)

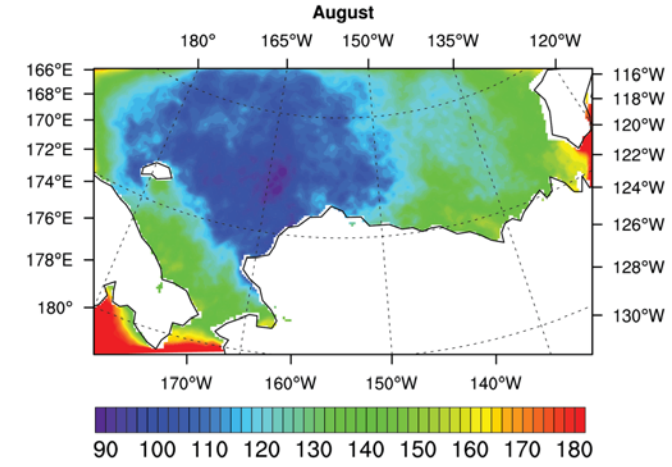

(b)

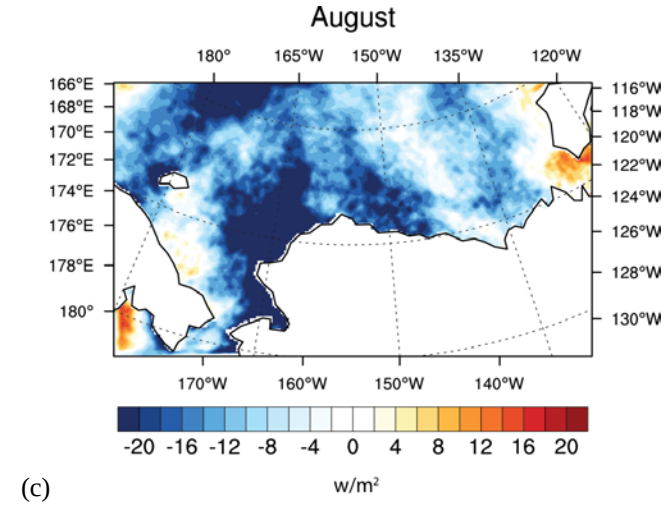

(c)

Figure 16. (a) Climatological and (b)W2E storm composite downward shortwave radiation. (c) Difference between the W2E storm composite and climatological downward shortwave radiation.

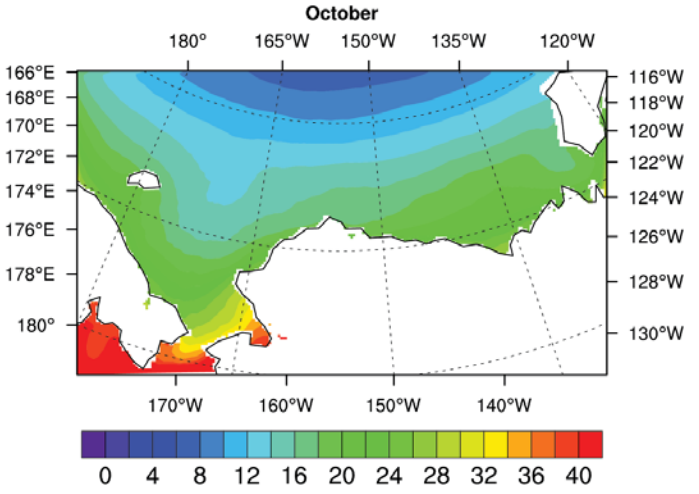

(a)

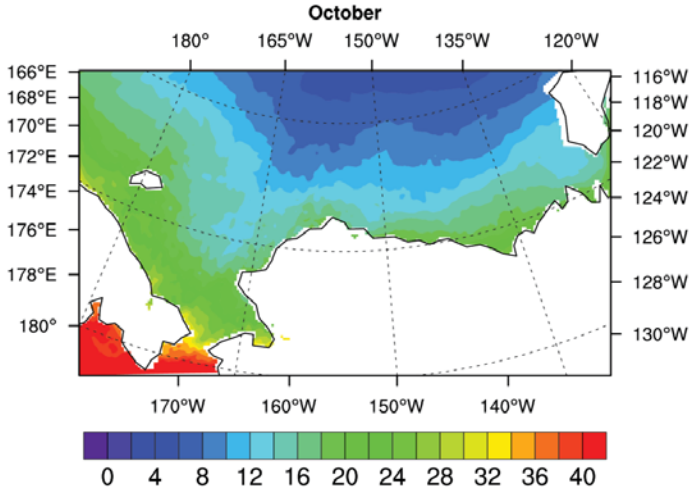

(b)

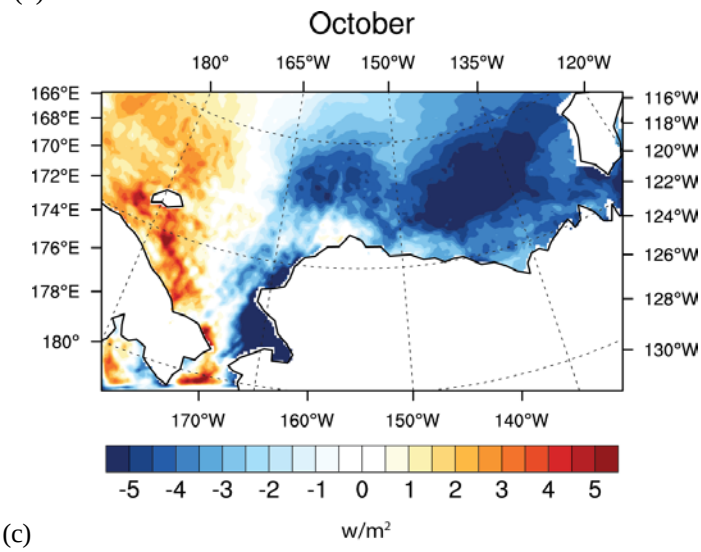

(c)

Figure 17. (a) Climatological and (b)S2NP storm composite downward shortwave radiation. (c) Difference between the S2NP storm composite and climatological downward shortwave radiation.

Surface sensible heat flux

The ocean transfers heat absorbed from both longwave and shortwave radiation into the atmosphere primarily by surface sensible and latent heat flux. Sensible heat is transported from warm to cold subjects. Sensible heat flux can be found when there are differences in temperature between the atmosphere and the ocean surface below. The values of the surface sensible flux are usually much smaller than the radiation terms. Summertime absorption of solar radiation in open water can melt sea ice and increase the surface sensible heat content of the upper ocean. In August, the climatological surface heat flux is upward (positive) in the southern Chukchi Sea over open water areas south of the sea ice margin where low albedo can promote strong solar heating and increase the oceanic sensible heat (Figure 18a). When the W2E storms occur, the upward sensible heat flux decreases most along the western coast of Alaska, the eastern coast of East Siberian Sea, and in the southern Chukchi Sea (Figures 18b and 18c). This corresponds to the region with the strongest southwesterly offshore wind, which can advect warm air from the East Siberian Sea to the Chukchi Sea. In October, S2NP storms reduce surface sensible heat flux (Figure 19) by increasing the 2 m surface air temperature in the southeastern Chukchi Sea and the southern Beaufort Sea (Figure 10b). Decreases of the sensible heat flux in the Bering Strait and along the coast of the East Siberian Sea can be affected by the decrease of SST in that region.

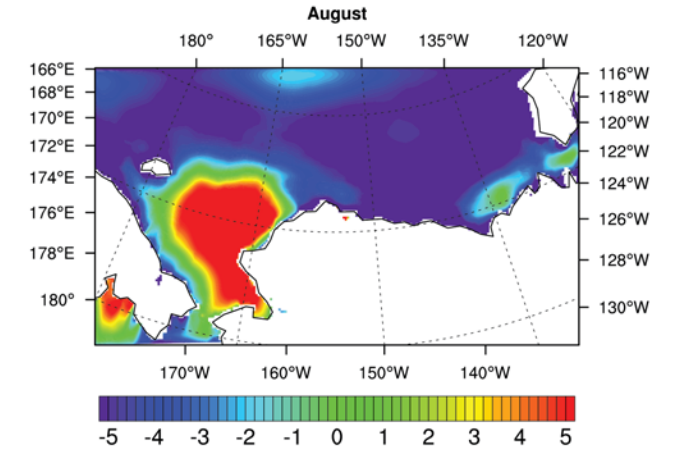

(a)

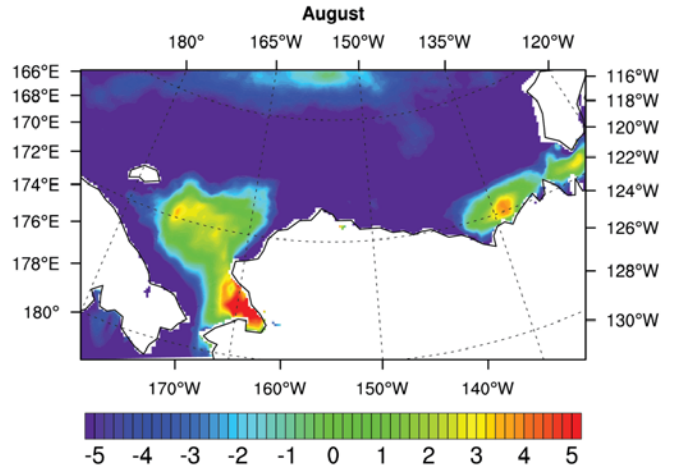

(b)

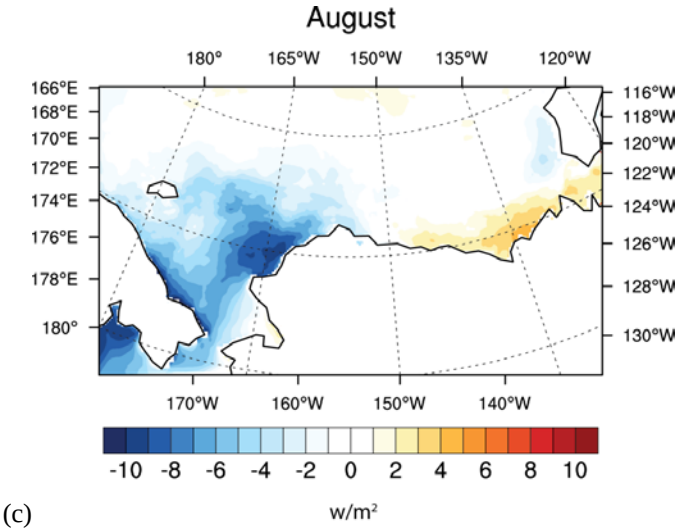

(c)

Figure 18. (a) Climatological and (b) W2E storm composite surface sensible heat flux. (c) Difference between the W2E storm composite and climatological surface sensible net heat flux.

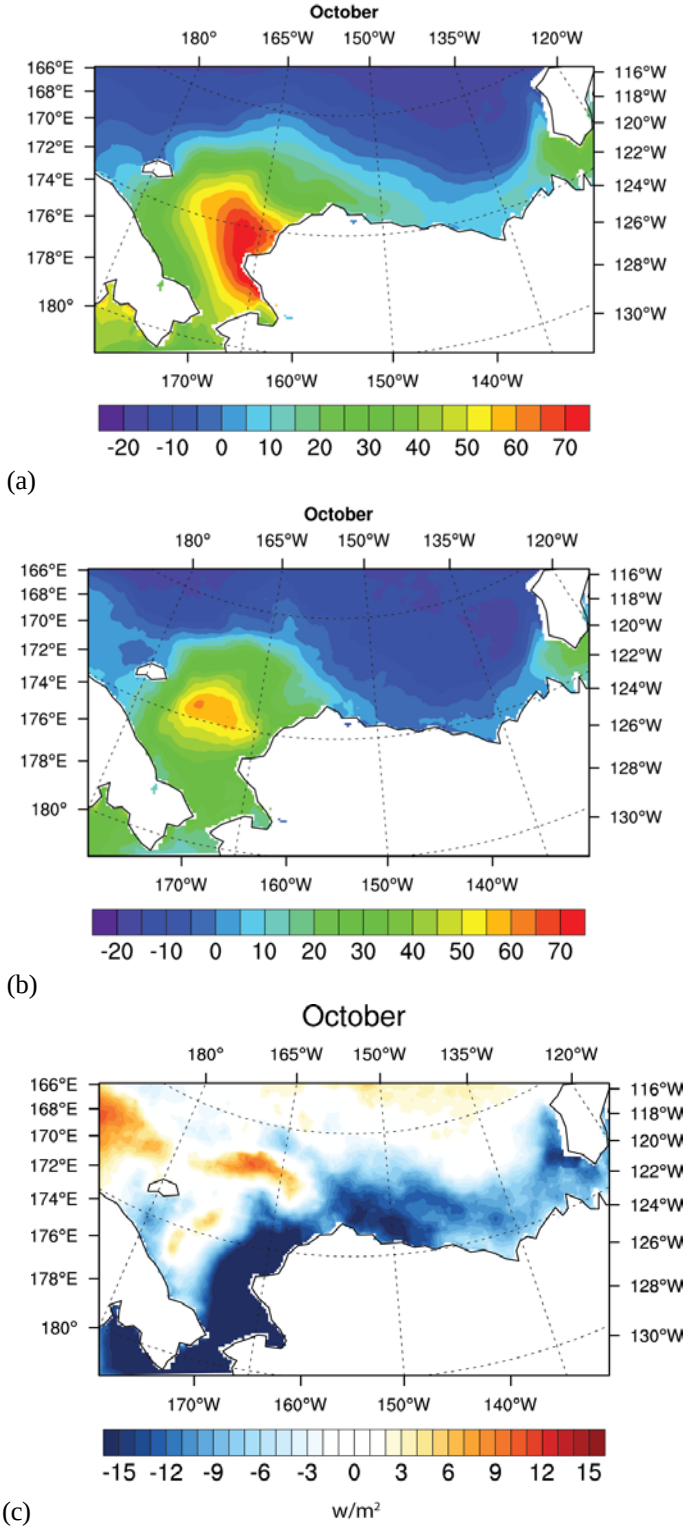

Figure 19. (a) Climatological and (b) S2NP storm composite surface sensible heat flux. (c) Difference between the S2NP storm composite and climatological surface sensible net heat flux.

Surface latent heat flux

We examined changes in surface latent heat flux linked to W2E and S2NP storm activity (Figures 20 and 21, respectively). In the Arctic, surface latent heat flux transfers of energy between ice and the atmosphere, i.e., when sea ice melts, latent heat is absorbed, and when sea ice forms, latent heat is released. Surface latent heat flux followed the same pattern as surface sensible heat flux; the maximum decrease caused by W2E storms occurred in August along the northwestern Alaska coast and East Siberian Sea coast (Figure 20c), and the maximum decrease caused by S2NP storms occurred in October along the Alaskan coast in the Chukchi and Beaufort Seas and in the Bering Strait (Figure 21c).

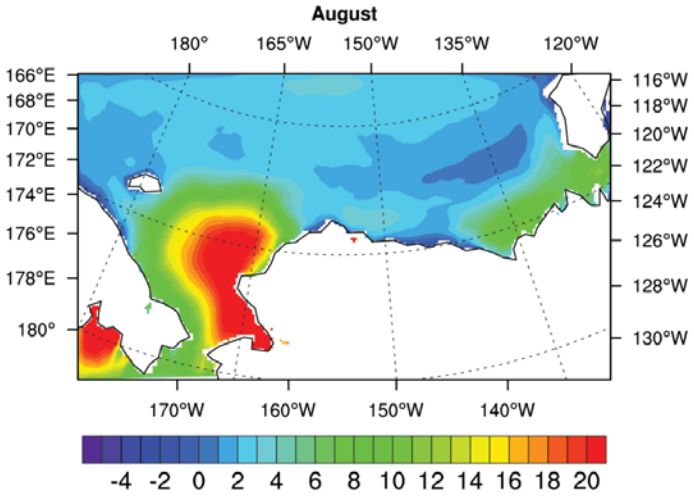

(a)

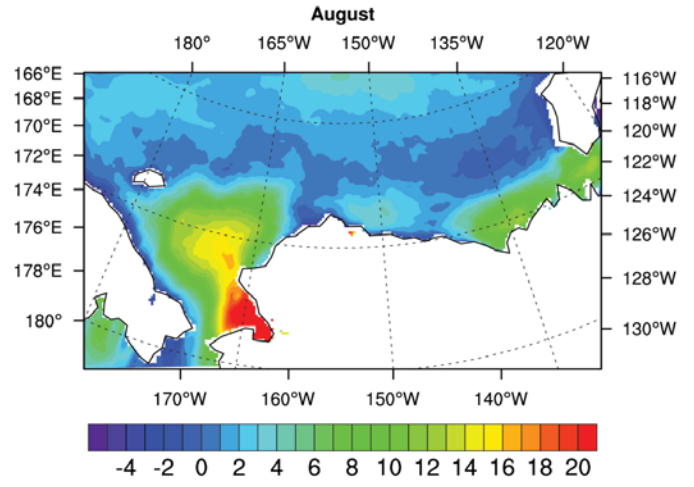

(b)

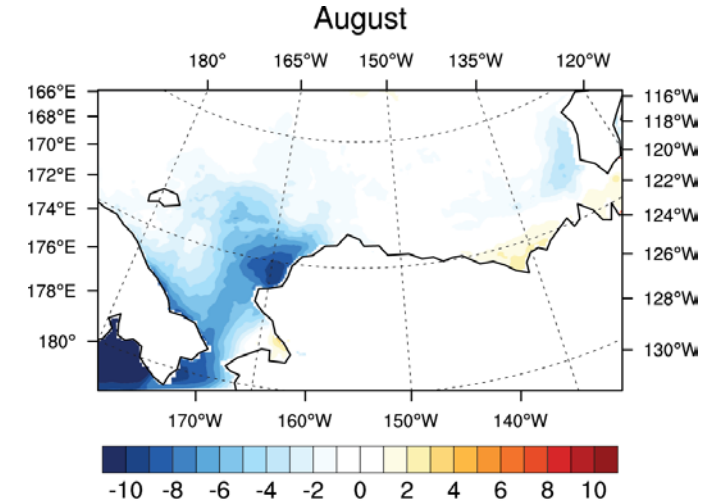

(c)

Figure 20. (a) Climatological and (b) W2E storm composite surface latent net heat flux. (c) Difference between the W2E storm composite and climatological surface latent net heat flux.

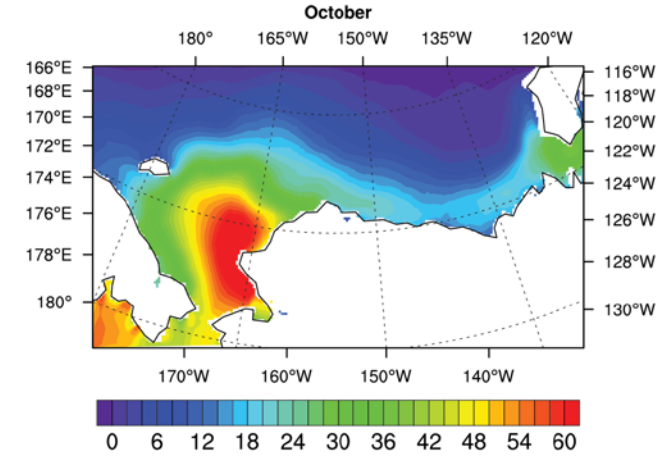

(a)

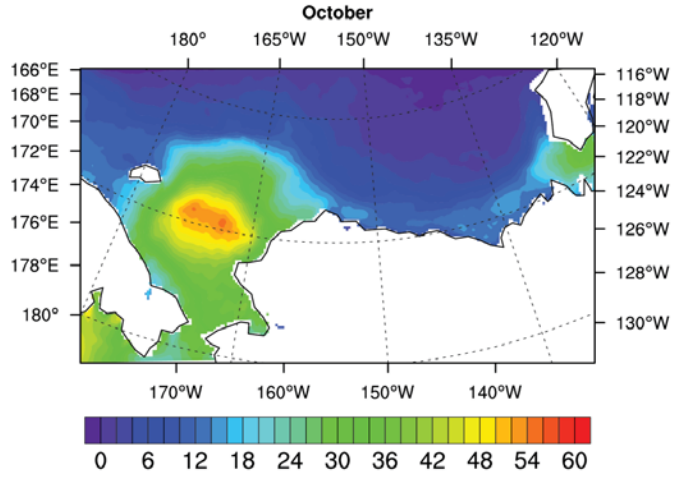

(b)

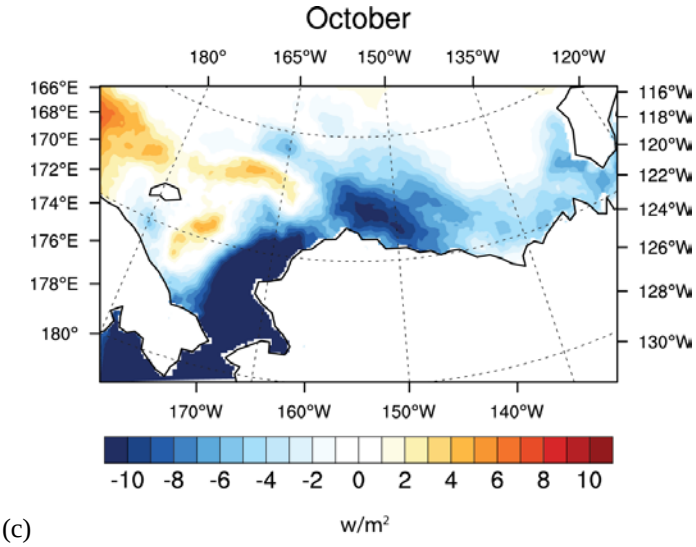

(c)

Figure 21. (a) Climatological and (b) S2NP storm composite surface latent net heat flux. (c) Difference between the S2NP storm composite and climatological surface latent net heat flux.

Conclusions

This study characterizes the climatology of the S2NP and the W2E storms and their impact on the ocean and regional climate. The W2E storms have a pronounced seasonal cycle with the highest intensity in August and lowest intensity in winter, while the S2NP storms occur more regularly throughout the year and reach the highest intensity in October. The S2NP storms in October are generally more intense than the W2E storms in August. Differences between the storm composite and climatological surface conditions are large and substantial. S2NP and W2E storms affect the Chukchi and Beaufort Seas surface climate. For example, the August W2E storms developed in the East Siberian Sea are associated with higher than normal southwesterly wind speed in the Bering Strait and the Chukchi Seas, which can advect warm continental air over the ocean and help melt the sea ice. The October S2NP storms can cause significant surface temperature increase over the eastern Chukchi Sea and change the prevailing easterly flow in the Beaufort Sea to southeasterly flow. The offshore flow associated with the S2NP winds can help push sea ice away from the coast and decrease the sea ice concentration. The W2E and S2MP storms both increase cloudiness and, accordingly, decreases in downward shortwave radiation decreases and increases in downward longwave radiation.

Acknowledgments

This study was funded by Coastal Marine Institute and Bureau of Ocean Energy Management, Alaska OCS Region. Special thanks go to Dr. Seth Danielson of College of Fisheries and Ocean Sciences at the University of Alaska Fairbanks for his insightful comments and review on this work. We also thank Dr. Jing Zhang of North Carolina A&T State University, who provided valuable information related to the CBHAR data. We would also like to express special thanks to Warren Horowitz, Project Officer, and Heather Crowley at BOEM for their excellent recommendations and feedback on the quarterly and final reports. We also thank and Guillermo Auad, who provided valuable recommendations and comments to the quarterly and final reports.

References

Comiso, J. C., C. L. Parkinson, R. Gersten, and L. Stock (2008), Accelerated decline in the Arctic sea ice cover. Geophys. Res. Lett., 35, L01703.

Dee, D. P., S. M. Uppala, A. J. Simmons, P. Berrisford, P. Poli, S. Kobayashi, U. Andrae, M. A. Balmaseda, G. Balsamo, P. Bauer, P. Bechtold, A. C. M. Beljaars, L. Van de Berg, J. Bidlot, N. Bormann, C. Delsol, R. Dragani, M. Fuentes, A. J. Geer, L. Haimberger, S. B. Healy, H. Hersbach, E. V. Hólm, L. Isaksen, P. Kållberg, M. Köhler, M. Matricardi, A. P. McNally, B. M. Monge-Sanz, J.-J. Morcrette, B.-K. Park, C. Peubey, P. De Rosnay, C. Tavolato, J.-N Thépaut, and F. Vitart (2011), The ERA-Interim reanalysis: Configuration and performance of the data assimilation system. Quart. J. Roy. Meteor. Soc., 137, 553–597. doi:10.1002/qj.828

Graham, R. M., L. Cohen, A. A. Petty, L. N. Boisvert, A. Rinke, S. R. Hudson, M. Nicolaus, and M. A. Granskog (2017), Increasing frequency and duration of Arctic winter warming events. Geophys. Res. Lett., 44, 6974–6983.

Liu F., J. R. Krieger, and J. Zhang (2014), Toward Producing the Chukchi–Beaufort High-Resolution Atmospheric Reanalysis (CBHAR) via the WRFDA Data Assimilation System. Mon. Wea. Rev., 142, 788–805.

Roeckner, E; G. Bäuml, L. Bonaventura, R. Brokopf, M. Esch, M. Giorgetta, S. Hagemann, I. Kirchner, L. Kornblueh, E. Manzini, A. Rhodin, U. Schlese, U. Schulzweida, and A. Tompkins (2003), The atmospheric general circulation model ECHAM5. Part 1. Model description. Report no. 349, Max-Planck-Institut für Meteorologie (MPI-M).

Rinke, A., R. Gerdes, K. Dethloff, T. Kandlbinder, M. Karcher, F. Kauker, S. Frickenhaus, C. Köberle, and W. Hiller (2003), A case study of the anomalous Arctic sea ice conditions during 1990: Insights from coupled and uncoupled regional climate model simulations. J. Geophys. Res., 108(D9), 4275. doi:10.1029/2002JD003146.

Rinke, A., K. Dethloff, W. Dorn, D. Handorf, and J. C. Moore (2013), Simulated Arctic atmospheric feedbacks associated with late summer sea ice anomalies. J. Geophys. Res. Atmos., 118, 7698–7714. doi:10.1002/jgrd.50584.

Screen, J. A., and I. Simmonds (2010), The central role of diminishing sea ice in recent Arctic temperature amplification. Nature., 464, 1334–1337.

Serreze, M. C. (1995), Climatological aspects of cyclone development and decay in the Arctic. Atmos.–Ocean., 33, 1–23.

Serreze, M. C., and A. P. Barrett (2008), The summer cyclone maximum over the central Arctic Ocean. J. Climate., 21, 1048–1065.

Skamarock, W. C., J. B. Klemp, J. Dudhia, D. O. Gill, D. M. Barker. M. G. Duda, X.-Y Huang, W. Wang, and J. G. Powers (2008), A description of the Advanced Research WRF version 3. NCAR Tech Note NCAR/TN–4751STR, 113 pp.

Simmonds, I., C. Burke, K. Keay (2008), Arctic climate change as manifest in cyclone behavior. J. Climate., 21, 5777–5796.

Simmonds, I., and I. Rudeva (2012), The great Arctic cyclone of August 2012. Geophys. Res. Lett., 39, L23709.

Steele, M., W. Ermold, and J. Zhang (2008), Arctic Ocean surface warming trends over the past 100 years. Geophys. Res. Lett., 35, L02614.

Undén, P; L. Rontu, H. Järvinen, P. Lynch, J. Calvo, G. Cats, J. Cuxart, K. Eerola, C. Fortelius, J. A. Garcia-Moya, C. Jones, G. Lenderlink, A. McDonald, R. McGrath, B. Navascues, N. Woetman, V. Ødegaard, E. Rodrigues, M. Rummukainen, R. Rõõm, K. Sattler, B. Hansen-Sass, H. Savijärvi, B. Wichers-Schreur, R. Sigg, H. The, and A. Tijm (2002), HIRLAM-5 Scientific Documentation. Scientific Report. http://hirlam.org.

Wendler, G. (1973), Sea ice observation by means of satellite. J. Geophys. Res., 78(9), 1427–1448.

Woods, C. and R. Caballero (2016), The Role of Moist Intrusions in Winter Arctic Warming and Sea Ice Decline. J. Climate., 29, 4473–4485.

Zhang, X., J. E. Walsh, J. Zhang, U. S. Bhatt, and M. Ikeda (2004), Climatology and interannual variability of Arctic cyclone activity 1948–2002. J. Climate., 17, 2300– 2317.

Zhang, X., J. Zhang, J. Krieger, M. Shulski, F. Liu, S. Stegall, W. Tao, J. You, and B. Potter, (2013), Beaufort and Chukchi Seas mesoscale meteorology modeling study. Final Project Report. Bureau of Ocean Energy Management, BOEM 2013-0119, 204 pp.

Using Genotyping-by-Sequencing (GBS) Population Genetics Approaches to Determine the Population Structure of Tanner Crab (*Chionoecetes bairdi*) in Alaska

Principal Investigator: Genevieve Johnson

College of Fisheries and Ocean Sciences
University of Alaska Fairbanks

Cooperative Agreement Number: M16AC00011
Period of Performance: 6/16-1/18

Contents

List of Figures and Tables

List of Tables

Abstract

Information on the extent of migration and structure of wild populations is an important consideration in the development of natural resource management policies. Genomic studies can increase our ability to the detect differences in population structure. Until recently, use of such studies was limited by the genomic resources and databases available for a particular species. However, novel and continuously refined sequencing technology offers the potential to circumvent this barrier and provide access to genomic-scale datasets of genetic variation, even for species without available reference genomes. This project focused on developing baseline estimates of the genome-wide variation and population structure of Tanner crab (*Chionoecetes bairdi*), a commercial species that is important to Alaska's economy and society. The Tanner crab is targeted in commercial, personal use, and subsistence fisheries in Alaska. Previously strong crab fisheries in Prince William Sound, Kodiak, and the Bering Sea have faced major uncertainties over the past few decades, including declines and mixed recoveries that may be linked to environmental changes and both anthropogenic and biological factors. Here, we attempted to apply genomic sequencing techniques to investigate the population structure of *C. bairdi* in Alaska, focusing on the connectivity of Cook Inlet and Shelikof Strait populations with populations in Southeast Alaska, Prince William Sound, Kodiak Island, the Alaska Peninsula, the Aleutian Islands, and the Bering Sea shelf. Technical issues limited the sample sizes from Southeast Alaska, Prince William Sound, and the Bering Sea shelf and restricted the geographical regions that could be statistically compared. No significant distinction between regions could be detected based on individuals' genotypes through measurements of F_{ST} or by Principal Components Analysis (PCA). We are continuing to test population structure models and estimates of genome-wide variation and diversity.

Introduction

An understanding of population boundaries is an important consideration in the development of natural resource management policies (Reiss et al. 2009; Webb & Woodby 2011). Determining these boundaries for marine organisms can pose a special challenge, particularly for species that disperse during pelagic larval life stages. Due to lack of observable physical boundaries and obstacles to migration in marine environments, it was long assumed that marine populations were largely homogenous (Caley et al., 1996). However, while marine populations may have less variation than freshwater species, which have obvious population barriers, studies have shown low-level variation and evidence of subpopulations in marine organisms (e.g., Ward et al., 1994; Merkouris et al., 1998; Hutchinson et al., 2001; Reiss et al., 2009). Even minor levels of differentiation can indicate a lack of connectivity between regions (Palumbi, 2003; Reiss et al., 2009). Physical mechanisms including tidal currents, water stratification, shore topography, wind, and other oceanographic features may affect larval dispersal and retention (Cowen & Sponaugle, 2009). In addition, biological constraints to successful larval propagation may also exist.

Tanner crab (*Chionoecetes bairdi)* is important species in commercial, personal use, and subsistence fisheries in Alaska. Tanner crab ranges from the southern Bering Sea across Southcentral Alaska to Southeast Alaska. Stocks throughout the Gulf of Alaska are managed by the Alaska Department of Fish and Game (ADF&G) (Otto & Pengilly 2002; Woodby et al. 2005) and stocks in the Bering Sea are jointly managed by ADF&G and the National Marine Fisheries Service (NMFS). The Bering Sea commercial fishery was once the most substantial crab fishery in the state by landed weight. The Prince William Sound fishery historically comprised the majority of shellfish harvested in the Gulf of Alaska region (NPFMC 2016; Trowbridge 1993). Tanner crab abundance has faced major declines, probably linked to environmental change among other factors (Armstrong et al. 1998; Zheng & Kruse 2006). Population recovery has been variable and is not well understood. More information on the genetic structure of Alaskan Tanner crab populations may help us understand the extent of migration and mixing across regions of Alaska and explain some of the variability observed in recovery. It is important to know whether Tanner crab stocks around Cook Inlet and Shelikof Strait (Bureau of Ocean Energy Management [BOEM] study areas) are isolated and distinct or substantially connected to other populations throughout Alaska. If the former is the case, management of offshore activities should address the potential of impacting an isolated stock that would not be supplemented by other populations. If the latter is the case, potential impacts from offshore activities might be mediated by recruits entering affected areas from elsewhere.

Genome sequencing tools are increasingly being applied to assess population structure and connectivity in marine species and have detected more complex spatial structures than previously identified (Jørstad, 2004; Hauser & Carvalho, 2008). Reduced-representation genome-wide scans involve simultaneous discovery and genotyping of hundreds to thousands of single nucleotide polymorphisms (SNPs). The datasets generated by these approaches are useful for resolving fine-

scale structure and detecting low levels of variation (Peterson et al. 2012; Rodrigues-Ezpeleta et al., 2015). Double-digest restriction-associated DNA sequencing (ddRAD) is a reduced-representation sequencing approach that samples a subset of regions rather than sequencing all regions of the entire genome. ddRAD sequencing provides a cost-effective way to analyze the genomes of non-model organisms with little reference data because deep coverage of reads can be obtained from genome regions adjacent to restriction-enzyme cut sites. Restriction-enzyme digestion is based on occurrences of restriction-enzyme recognition sites that are relatively consistent throughout the genomes of closely related individuals, so there is no primer-identification step required (Peterson et al. 2012).

Here, we applied these techniques to investigate the population structure of *C. bairdi* in Alaska, focusing on the connectivity of Cook Inlet and Shelikof Strait populations with populations in Southeast Alaska, Prince William Sound, Kodiak Island, the Alaska Peninsula, the Aleutian Islands, and the Bering Sea shelf. This study will increase our understanding of marine organisms that could be affected by offshore development activities. Insight into population genetic structure may be able to uncover multi-generational movement patterns that are not otherwise distinguishable and may indicate why the stock abundances are so variable.

Objectives

1. Test the null hypothesis of genetic homogeneity across all sampled populations using an extensive multi-locus genotype dataset. If genetic heterogeneity is detected, test alternative models of population structure.

2. Assess whether populations in BOEM special project areas of Cook Inlet and Shelikof Strait are distinct or contiguous with nearby populations and assess the extent of their natural genetic variability.

3. Test for evidence of extreme population size changes in the extent and nature of observed standing genetic variation.

Methods

Sample Collection

From 2009–2016, a total of 1204 *C. bairdi* crabs were sampled over nine regions including Southeast Alaska, Prince William Sound, Kachemak Bay, Shelikof Strait, Kodiak Island, the Alaska Peninsula, the Aleutian Islands, the Bering Sea west of 166°W, and the Bering Sea east of 166°W (Figure 1). Crabs were collected by pots or trawl during annual stock assessment surveys conducted by NMFS and ADF&G. Samples of tissue (dactyl segment of walking leg) or hemolymph (0.2 mL) were stored in 95–100% ethanol at -15°C. A subset of these samples (~28 per region) was selected for DNA extraction and sequencing. Sampling efforts were not uniform across regions, so each region was treated as a cluster and samples were selected systematically to get approximately uniform coverage across each geographic region. An additional ten Beaufort Sea *C. opilio* samples were sequenced to detect introgression and to use as an outgroup.

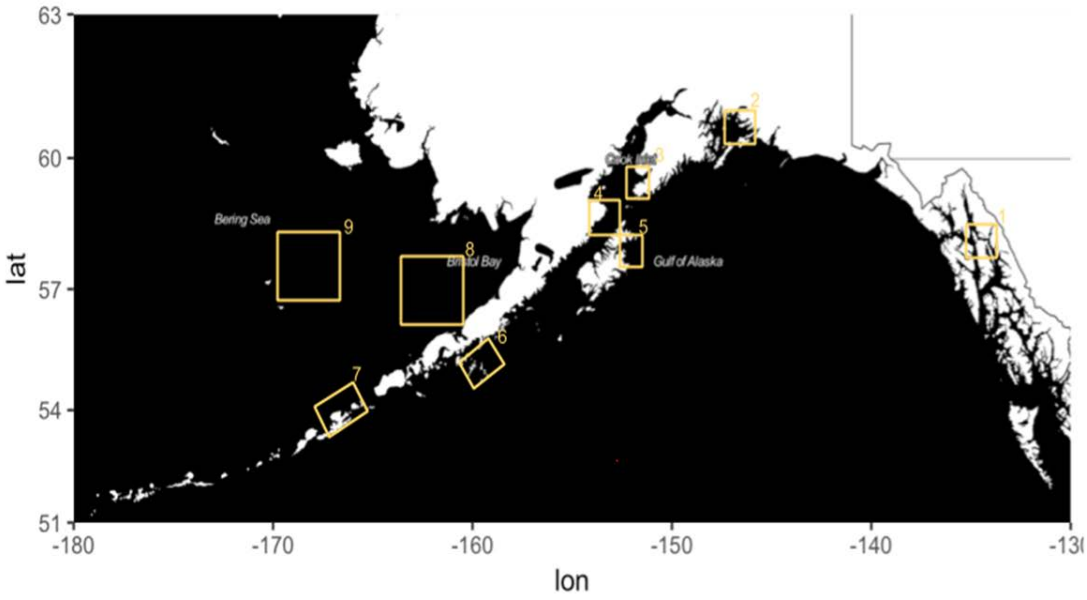

Figure 1. Map of sampling regions. Southeast Alaska (1), Prince William Sound (2), Kachemak Bay (3), Shelikof Strait (4), Kodiak Island (5), Alaska Peninsula (6), Aleutian Islands (7), SE eastern Bering Sea (8), and NW eastern Bering Sea (9).

DNA Extraction, ddRAD Library Preparation, and Sequencing

Total genomic DNA was extracted using the Gentra Puregene Tissue Kit by QIAGEN (QIAGEN, Valencia, CA, USA). DNA extractions were assessed for quality (long fragment lengths) by gel electrophoresis. DNA quantity and protein contamination were checked with a Qubit 2.0 fluorometer and a Nanodrop 1000 spectrophotometer, respectively.

Samples were processed according to the double-digest restriction-associated DNA (ddRAD) sequencing protocol developed by Peterson et al., 2012 (Figure 2). This method allocates sequencing effort to a subset of restriction digest fragments and ensures that the same genomic regions or loci are sequenced from the different individuals being genotyped. DNA extracts were sent to Research and Testing Laboratory (RTL; Lubbock, TX, USA) and Admera Health (South Plainfield, NJ, USA) for digestion, size selection, library preparation, and sequencing. Genomic DNA from each sample was fragmented using a combination of restriction enzymes (EcoRI-HF and MspI) to generate pools of variable length fragments flanked by the restriction-enzyme recognition sites. The tagged genomic fragment pools were size selected at 350–400 bp, using a BluePippin (Sage Science, Beverly, MA, USA). The size-selected pools were then sequenced on an Illumina Hi-Seq platform (Illumina Inc, San Diego, CA, USA) to generate >1 million sequence reads from each individual.

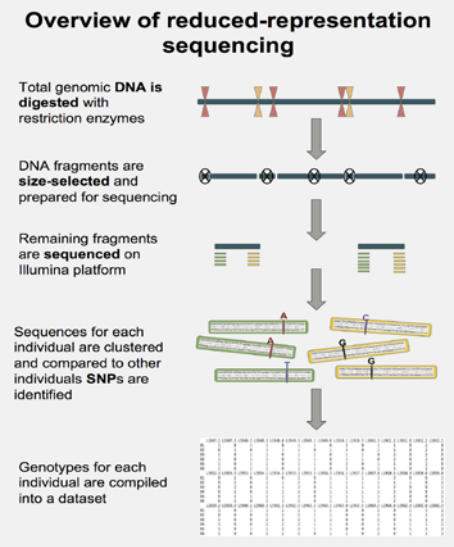

Figure 2. A representation of ddRAD sequencing method.

Read Filtering, SNP Calling, and Genotype Assembly

Demultiplexed FASTQ files were run through *FASTQC* (Andrews, 2010) to assess overall sequence quality and to obtain summary statistics. On average, the sequence quality dropped below moderate thresholds for the last 20 bases of each read, so reads were trimmed by 20 bp from the 3' end during the second step of assembly in the ipyrad toolkit (Eaton, 2016). The demultiplexed FASTQ reads were filtered, clustered, and aligned in ipyrad in order to call variant sites and assemble a dataset of individual genotypes. A range of inputs for the parameters of minimum read depth and clustering thresholds were tested to check for potential bias in SNP calls.

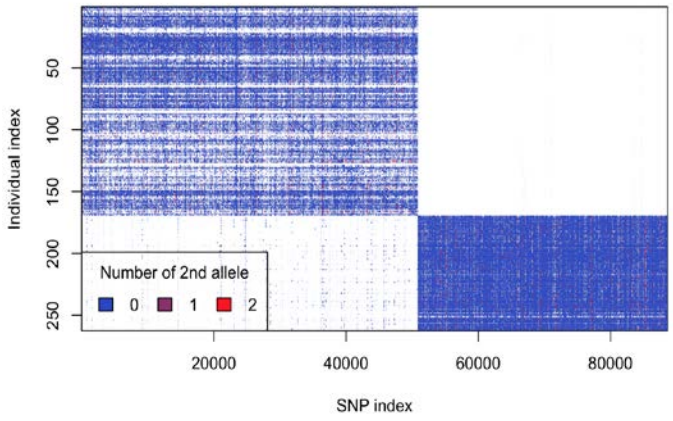

Figure 3. Plot of locus coverage across individuals. The x-axis represents all loci that were retained in the final genotype assembly. The y-axis represents each individual that was genotyped. Along the y-axis, the lower 100 individuals were part of the library preparation and sequencing serviced by RTL Genomics. The upper 170 individuals were part of the set of samples that were serviced by Admera Health. Very few loci were genotyped across both groups.

Genetic Diversity and Population Genetic Analyses

Genotype assemblies were added using the vcfR package (Knaus & Grunwald, 2016). The adegenet package (Jombart & Ahmed, 2011) was used to plot summary information for genotype assemblies and perform Principal Components Analysis (PCA) on SNPs to identify potential clustering patterns among individuals. We also used it to calculate heterozygosity within individuals, subpopulations, and within the total population. F_{IS} and F_{ST} were calculated according to the Weir & Cockerham (1984) method implemented in hierfstat (Goudet, 2005).

Results

Of the 100 DNA extraction samples that were processed and sequenced by RTL Genomics, 93 individual samples yielded >0.5 M reads. The ddRAD libraries from the seven individuals that had <0.5 M were sequenced again but failed to meet the 0.5 M threshold and were dropped from the analysis. After quality filtering, reads per individual in the final dataset ranged 605,824 – 4,793,785 with an average of 1,897,727. On average, only 0.88% of reads were filtered out due to low quality.

Our overall dataset was compromised because very few loci were genotyped across all samples. By looking at the locus coverage plot (Figure 3), it is apparent that there was a strong discrepancy between loci that were recovered from the samples processed by RTL Genomics and those processed by Admera Health. Due to uncontrollable circumstances, we were not able to work with the same sequencing provider for all stages of this project. Although we specified particular restriction enzymes and size-selection thresholds for each service provider, minor differences in instruments or site-specific protocols may have led to this issue of locus coverage bias. Since the datasets do not overlap, we analyzed each group separately. From this point on, we refer to the samples that were processed by RTL Genomics as "Set 1." Set 1 was composed of 25 individuals from Southeast Alaska, 25 individuals from Prince William Sound, 25 individuals from the SE eastern Bering Sea, and 25 individuals from the NW eastern Bering Sea. We refer to the samples processed by Admera Health as "Set 2." Set 2 samples consisted of 28 individuals from Kachemak Bay, 28 individuals from Shelikof Strait, 28 individuals from the Alaska Peninsula, 28 individuals from the Aleutian Islands, 28 individuals from Kodiak Island, 5 individuals from the NW eastern Bering Sea, 4 individuals from the SE eastern Bering Sea, 7 individuals from Prince William Sound, 4 individuals from Southeast Alaska, and 10 *C. opilio* samples from the Beaufort Sea.

F_{ST} is a measure of variation within a subpopulation relative to the total. A value close to zero indicates high connectivity between regions or large populations with several migrants. As values approach one, they indicate more isolated populations, with less migration between the subpopulations. None of the populations included in Set 1 had large F_{ST} values, indicating that there is some connectivity between the regions (Table 1).

Table 1. Pairwise genetic distance calculations for Set 1, based on Weir & Cockerham F_{ST} (Weir & Cockerham, 1984).

	EBS_NW	EBS_SE	PWS
EBS_SE	0.0005085823		
PWS	0.0058412348	0.0050166246	
SEAK	-0.0022553837	0.0058942658	0.0019089325

All of the regions in Set 2 showed some differentiation from the *C. opilio* samples from the Beaufort, with the Bering Sea paired samples having the lowest F_{ST} values (Table 2). This is expected because there is hybridization between *C. opilio* and *C. bairdi* in the Bering Sea. It is important to note that the Set 2 sample sizes from Southeast Alaska, Prince William Sound, SE eastern Bering Sea, and NW eastern Bering Sea were not large enough to make accurate comparisons. All of the pairwise F_{ST} values between Set 2 regions with adequate sample sizes were close to zero, indicating substantial population connectivity.

Table 2. Pairwise genetic distance calculations for Set 2, based on Weir & Cockerham F_{ST} (Weir & Cockerham, 1984).

	Beaufort	EBS_NW	EBS_SE	KBay	Shelikof	Kodiak	AKpen	Aleutian	PWS
EBS_NW	-0.009667613								
EBS_SE	0.027705318	-0.18514276							
KBay	0.469531293	0.286409066	0.24392811						
Shelikof	0.467471239	0.282299457	0.23903579	-0.0026346198					
Kodiak	0.467133515	0.283081511	0.24737442	0.0005767091	0.0021622383				
AKpen	0.47297505	0.291525695	0.24680543	-0.0010437049	-0.0014327386	-0.0025865687			
Aleutian	0.471789604	0.286322364	0.24465215	-0.0007037092	-0.0011546424	0.0019111874	-0.0001890493		
PWS	0.41211025	0.208712148	0.20543012	0.0041447305	0.0044290488	0.0110118635	0.0042518539	-0.0010508976	
SEAK	0.370109603	0.165464122	0.1714497	0.0020573475	0.0007170724	0.0034855329	0.0057633322	0.0043821051	0.009953875

PCA plots (Figures 4–6) demonstrate the lack of strong population genetic structure. The *C. opilio* samples showed greater diversity and did not cluster strongly with the *C. bairdi* samples. This indicates high gene flow or very low genetic diversity between our regions.

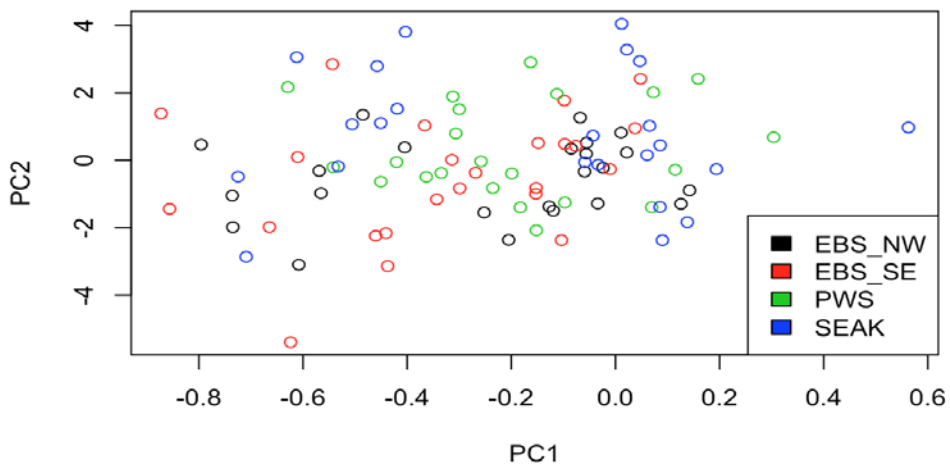

Figure 4. Set 1 PCA plot of first and second principal components using the adgenet (Jombart, 2008) package in R. Points are colored according to collection region. There is no clear grouping, and no patterns emerged amongst these regions based on this result.

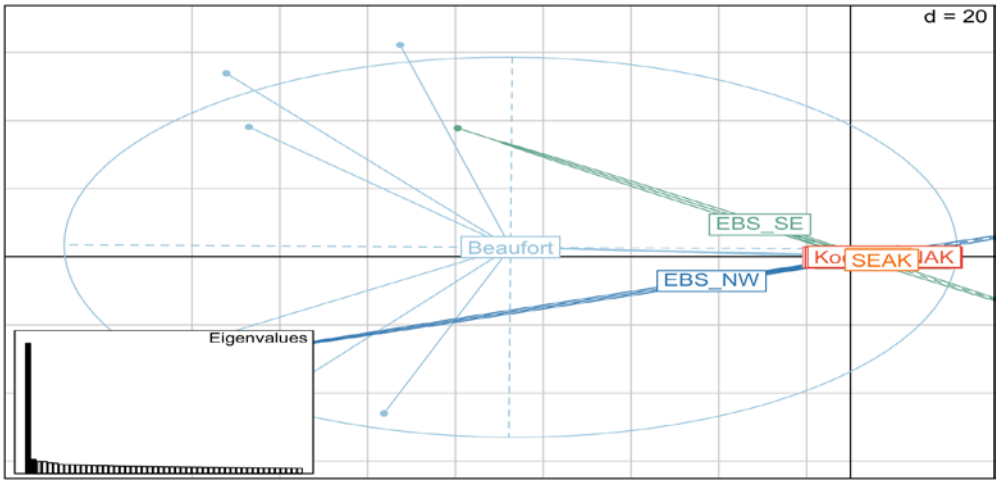

Figure 5. Set 2 PCA plot using the adgenet (Jombart, 2008) package in R. Points are colored according to collection region, and eclipses are drawn around groups. The Beaufort samples are *C. opilio*. We expect them to cluster away from the *C. bairdi* samples.

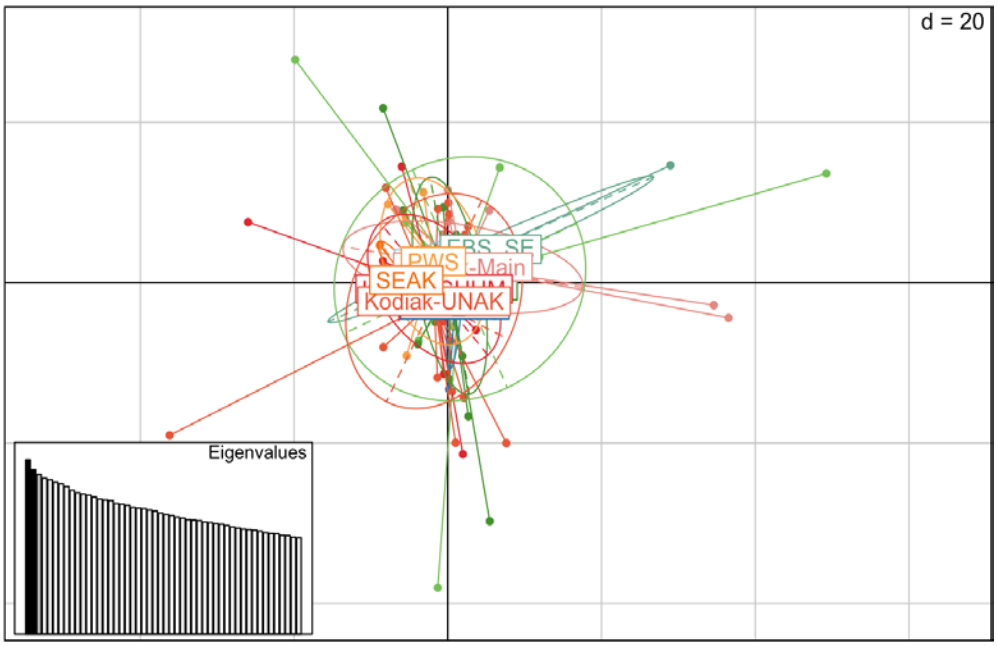

Figure 6. Set 2 PCA plot, with *C. opilio* removed, using the adgenet (Jombart, 2008) package in R. Points are colored according to collection region, and eclipses are drawn around groups. There is no clear grouping, and no patterns emerged amongst these regions based on this result.

Discussion

Instances of bias in locus coverage across multiple library preparation events have been reported (DaCosta & Sorenson, 2014) but not to this scale. The stark contrast in locus coverage across the samples from this project (Figure 3) could be due to offsets in size-selection specificity or an incorrect enzyme pair used in library preparation. We are following up with the service providers to check for errors in protocols.

When calling SNPs on datasets that contained samples from the Bering Sea, we observed a frequency distribution of SNPs-per-locus that was indicative of a recent mixing between two historically isolated groups (Travis Glenn University of Georgia, personal communication). These results are likely due to hybridization between *C. opilio* and *C. bairdi* in the Bering Sea and introgressed *C. opilio* alleles observed in our Bering Sea samples. The frequency distribution of SNPs-per-locus from a dataset of only Southeast Alaska samples does not produce this same pattern, indicating that introgressed *C. opilio* alleles are not prevalent in Gulf of Alaska samples. This is consistent with the introgression patterns noted by Merkouris et al. (1998). It also supports the idea that population connectivity is closely tied with larval advection in the direction of the Alaska Coastal Current and not against it. We plan to explore the extent of this hybridization in greater detail by characterizing variants that are exclusively characteristic of each species.

Pairwise F_{ST} estimates between regions indicated that there is gene flow. We are further characterizing this connectivity by testing models of isolation by distance and comparing directional migration estimates. We are testing other methods to investigate the genetic population structure. Moving forward, we plan to use Bayesian methods in *STRUCTURE* (Pritchard et al., 2003) to determine the number of subpopulations and perform assignment tests on individuals. Thus far, we are not able to reject the null hypothesis of our first objective, homogeneity across the populations, and there is not sufficient evidence of distinct populations in the study areas to address our second objective. These results may change or be clarified once we can pool together Set 1 and Set 2 data. The low levels of variation we observed could provide support for our third hypothesis, historical bottleneck or selection events, but they have not been statistically confirmed. Based on these initial analyses, the genome of *C. bairdi* is characterized by low levels of variation, and there are no clear differences in variation between regions across Alaska.

These results are not consistent with existing estimates of low but significant genetic differentiation among *C. bairdi* subpopulations detected with allozyme markers (Merkouris et al., 1998); however, we made comparisons at a different spatial scale. We only compared genetic diversity at the regional scale of our nine sampling regions, and our estimates suggest gene flow between each pair of regions. We did not pool the data over a larger regional scale (i.e., Southeast Alaska, Gulf of Alaska, and Bering Sea) as Merkouris et al. (1998) did. We also had an estimate of moderate to high gene flow between the northwest and southeast eastern Bering Sea regions. This does not align with previous allozyme findings or current models of larval advection patterns of *C. bairdi* in the eastern Bering Sea, which indicate some isolation in the southeast region near Bristol Bay (Merkouris et al., 1998; Richar et al., 2015). Our observations are more similar to the panmictic genetic population structure observed in *C. opilio* throughout Alaska (Albrecht et al., 2012). Additional analyses should help us determine which framework best represents the Tanner crab genetic population structure in the Bering Sea.

Acknowledgments

This research was supported by the University of Alaska Coastal Marine Institute (CMI) with funds from the Bureau of Ocean Energy Management (cooperative agreement M16AC00011). Funds were matched by the University of Alaska Fairbanks. Research reported in this publication was supported by the National Institute of General Medical Sciences of the National Institutes of Health under Award Numbers UL1GM118991, TL4GM118992, or RL5GM118990. The content is solely the responsibility of the authors and does not necessarily represent the official views of the National Institutes of Health. Collections for this project were supported by the Alaska Department of Fish and Game (Permit No. CF-16-102) and the National Marine Fisheries Service. The content is solely the responsibility of the authors and does not necessarily represent the official views of the ADF&G or NMFS. Thesis committee members included J. Andrés López, Ph.D.; Sarah Hardy, PhD.; and Ginny Eckert, Ph.D.

References

Albrecht, G. T., Valentin, A. E., Hundertmark, K. J., & Hardy, S. M. (2014). Panmixia in Alaskan populations of the snow crab *Chionoecetes opilio* (Malacostraca: Decapoda) in the Bering, Chukchi, and Beaufort Seas. Journal of Crustacean Biology, 34(1), 31–39.

Andrews, S. (2010). FastQC: A quality control tool for high throughput sequence data. Babraham Institute, Cambridge, UK.

Armstrong, J., Armstrong, D., & Hilborn, R. (1998). Crustacean resources are vulnerable to serial depletion–the multifaceted decline of crab and shrimp fisheries in the Greater Gulf of Alaska. Reviews in Fish Biology and Fisheries, 8(2), 117–176.

Caley, M. J., Carr, M. H., Hixon, M. A., Hughes, T. P., Jones, G. P., & Menge, B. A. (1996). Recruitment and the local dynamics of open marine populations. Annual Review of Ecology and Systematics, 477–500.

Cowen, R. K., & Sponaugle, S. (2009). Larval dispersal and marine population connectivity. Annual Review of Marine Science V1, 443–466.

DaCosta, J. M., & Sorenson, M. D. (2014). Amplification biases and consistent recovery of loci in a double-digest RAD-seq protocol. PLoS One, 9(9), e106713.

Eaton, D. (2016). ipyrad documentation. http://ipyrad.readthedocs.io/index.html

Goudet, J. (2005). Hierfstat, a package for R to compute and test hierarchical F-statistics. Molecular Ecology Resources, 5(1), 184–186.

Hauser, L., & Carvalho, G. R. (2008). Paradigm shifts in marine fisheries genetics: ugly hypotheses slain by beautiful facts. Fish and Fisheries, 9(4), 333–362.

Hutchinson, W. F., Carvalho, G. R., & Rogers, S. I. (2001). Marked genetic structuring in localized spawning populations of cod *Gadus morhua* in the North Sea and adjoining waters, as revealed by microsatellites. Marine Ecology Progress Series, 223, 251–260.

Jombart, T., & Ahmed, I. (2011). adegenet 1.3-1: new tools for the analysis of genome-wide SNP data. Bioinformatics, 27(21), 3070–3071.

Jørstad, K. E. (2004). Evidence for two highly differentiated herring groups at Goose Bank in the Barents Sea and the genetic relationship to Pacific herring, *Clupea allasi*. Environmental Biology of Fishes, 69(1–4), 211–221.

Knaus, B. J., & Grunwald, N. J. (2016). VcfR: an R package to manipulate and visualize VCF format data. bioRxiv, 041277.

Merkouris, S. E., Seeb, L. W., & Murphy, M. C. (1998). Low levels of genetic diversity in highly exploited populations of Alaskan Tanner crabs, *Chionoecetes bairdi*, and Alaskan and Atlantic snow crabs, *C. opilio*. Fishery Bulletin: National Oceanic and Atmospheric Administration, 96, 525–537.

North Pacific Fishery Management Council (NPFMC). (2016). 2016 Crab SAFE. Contributors: The Plan Team for the King and Tanner Crab Fisheries of the Bering Sea and Aleutian Islands, Bush, K., Dorn, M., Eckert, G., Foy, R.J., Garber-Yonts, B., Hamazaki, T., Ianelli, J. N., Punt, A.E., Rugolo, L., Siddeek, M.S.M., Stockhausen, W., Slater, L., Stram, D., Szuwalski, C., Turnock, B. J., Weber, D., & Zheng, J.

Otto, R. S., & Pengilly, D. (2002). Spatiotemporal trends in Tanner crab (*Chionoecetes bairdi*) size at maturity. Crabs in cold water regions: biology, management, and economics. A. J. Paul, E. G. Dawe, R. Elner, G. S. Jamieson, G. H. Kruse, R. S. Otto, B. Sainte-Marie, T. C. Shirley, and D. Woodby (eds.). University of Alaska Sea Grant, AK-SG, 02-01.

Palumbi, S. R. (2003). Population genetics, demographic connectivity, and the design of marine reserves. Ecological Applications, 13(1) Supplement, S146–S158.

Peterson, B. K., Weber, J. N., Kay, E. H., Fisher, H. S., & Hoekstra, H. E. (2012). Double digest RADseq: an inexpensive method for de novo SNP discovery and genotyping in model and non-model species. PLoS One, 7(5), e37135.

Pritchard, J. K., Wen, W., & Falush, D. (2003). Documentation for structure software: version 2.

Reiss, H., Hoarau, G., Dickey-Collas, M., & Wolff, W. J. (2009). Genetic population structure of marine fish: mismatch between biological and fisheries management units. Fish and Fisheries, 10(4), 361–395.

Richar, J. I., Kruse, G. H., Curchitser, E., & Hermann, A. J. (2015). Patterns in connectivity and retention of simulated Tanner crab (*Chionoecetes bairdi*) larvae in the eastern Bering Sea. Progress in Oceanography, 138, 475–485.

Rodríguez-Ezpeleta, N., Bradbury, I. R., Mendibil, I., Álvarez, P., Cotano, U., & Irigoien, X. (2016). Population structure of Atlantic mackerel inferred from RAD-seq-derived SNP markers: effects of sequence clustering parameters and hierarchical SNP selection. Molecular Ecology Resources, 16(4), 991–1001.

Trowbridge, C. E. (1993). Prince William Sound Management Area 1992 Shellfish Annual Management Report. Alaska Division of Commercial Fisheries, Central Region.

Ward, R. D., Woodwark, M., & Skibinski, D. O. F. (1994). A comparison of genetic diversity levels in marine, freshwater, and anadromous fishes. Journal of Fish Biology, 44(2), 213–232.

Webb, J. B., & Woodby, D. (2011). Long-term Alaska crab research priorities, 2011. Alaska Department of Fish and Game, Division of Commercial Fisheries, Regional Information Report 5J11-04, Juneau, AK.

Weir, B. S., & Cockerham, C. C. (1984). Estimating F-statistics for the analysis of population structure. Evolution, 38(6), 1358–1370.

Woodby, D., Carlile, D., Siddeek, S., Funk, F., Clark, J. H., & Hulbert, L. (2005). Commercial fisheries of Alaska. Alaska Department of Fish and Game, Special Publication, (05–09), 74 pp.

Zheng, J., & Kruse, G. H. (2006). Recruitment variation of eastern Bering Sea crabs: Climate-forcing or top-down effects? Progress in Oceanography, 68(2), 184–204.

The Department of the Interior Mission

As the Nation's principal conservation agency, the Department of the Interior has responsibility for most of our nationally owned public lands and natural resources. This includes fostering the sound use of our land and water resources, protecting our fish, wildlife and biological diversity; preserving the environmental and cultural values of our national parks and historical places; and providing for the enjoyment of life through outdoor recreation.The Department assesses our energy and mineral resources andworks to ensure that their development is in the best interests of all our people by encouraging stewardship and citizen participation in their care. The Department also has a major responsibility for American Indian reservation communities and for people who live in island communities.

The Bureau of Ocean Energy Management

The Bureau of Ocean Energy Management (BOEM) works to manage the exploration and development of the nation's offshore resources in a way that appropriately balances economic development, energy independence, and environmental protection through oil and gas leases, renewable energy development and environmental reviews and studies.

The Department of the Interior Mission

As the Nation's principal conservation agency, the Department of the Interior has responsibility for most of our nationally owned public lands and natural resources. This includes fostering the sound use of our land and water resources, protecting our fish, wildlife and biological diversity; preserving the environmental and cultural values of our national parks and historical places; and providing for the enjoyment of life through outdoor recreation.The Department assesses our energy and mineral resources andworks to ensure that their development is in the best interests of all our people by encouraging stewardship and citizen participation in their care. The Department also has a major responsibility for American Indian reservation communities and for people who live in island communities.

The Bureau of Ocean Energy Management

The Bureau of Ocean Energy Management (BOEM) works to manage the exploration and development of the nation's offshore resources in a way that appropriately balances economic development, energy independence, and environmental protection through oil and gas leases, renewable energy development and environmental reviews and studies.